ABSTRACT

Title of thesis: PHYSICAL CHARACTERIZATION OF DNA CONDENSED WITH CATIONIC AGENTS

Eddy Salgado, Master of Science, 2016

Thesis directed by: Professor Robert M. Briber
Materials Science and Engineering

Gene therapy using non viral vectors remains a challenging problem of maximizing efficiency while minimizing risks due to the multiple biological hurdles for a carrier agent to deliver its genetic cargo. The precise connection between the physical properties of the vectors and their transfection behaviors remains to be fully realized. We have used atomic force microscopy as well as dynamic light scattering and zeta potential measurements in order to image and characterize DNA complexes with polyethylenimine (PEI), histidine-lysine (HK) peptide, and triethylenetetramine (TETA)-functionalized gold nanoparticles. The resulting complex structures are analyzed as a function of amine to phosphate (N/P) ratios and as a function of sample preparation protocols. This work aims to not only characterize these specific complexes, but to aid in the general understanding of complex formation and how it relates to transfection observations to promote a more rational design of future gene delivery agents.

PHYSICAL CHARACTERIZATION OF DNA CONDENSED WITH CATIONIC AGENTS

by

Eddy Salgado

Thesis submitted to the Faculty of the Graduate School of the
University of Maryland, College Park, in partial fulfillment
of the requirements for the degree of
Master of Science
2016

Advisory Committee:
Professor Robert M. Briber, Chair
Associate Professor Isabel K. Lloyd
Professor Peter Kofinas

Acknowledgements

First I would like to thank my former advisor Dr. Joonil Seog for the many hours of fruitful discussions, asking tough questions, and helping me become a more critical thinker along the way. Also, my current advisor Professor Robert Briber for the guidance and direction needed for this work.

I would also like to acknowledge all my fellow lab members who helped provide stimulating discussions during our group meetings and for a pleasant, knowledgeable atmosphere. Special thanks to Nitinun Varongchayakul for the initial AFM training, and Brian Stock for further discussions and mutual improvement of our AFM technique along the way. Lastly, I want to thank the undergraduates Jacob Hebert and Mariana Coelho for all their hard work and assistance in analyzing the data.

Finally, I would like to thank Professors Peter Kofinas and Isabel Lloyd for serving on my committee. I'd also like to thank them as well as their group members and Briber's group members who participated in the joint group meetings for the helpful questions and critique which has greatly shaped my oral presentation skills.

Table of Contents

List of Figures

Chapter 1: Background

1.1 Electrostatic DNA condensation

The DNA double helix structure is a very stiff polymer with a high persistence length as well as a highly charged polyelectrolytes. Despite this, DNA is regularly packaged into a tiny volume such as the nucleus of a cell or the compartment of a virus. In humans, the volume reduction due to the packing and organization of DNA is about four orders of magnitude [1]. Gene therapy, which involves the transfer of genetic material to cells, often requires artificial packing or condensation of DNA into carrier agents. It is therefore of great interest to understand the mechanisms that drive DNA condensation and how it can be controlled.

Double stranded DNA carries a charge of $-2e$ per base pair due to the phosphate groups on the backbone. Its persistence length is approximately 50 nm in physiological conditions. The persistence length is a measure of stiffness, defined as a characteristic length scale where the correlation of the tangential directions falls off by a factor of e. It has been estimated that the contribution to the persistence length from the repulsive electrostatic interactions along the DNA is roughly equal to the contribution due to stacking interactions between base pairs along the double helical structure [2], [3]. The stiffness can therefore be significantly reduced through electrostatic interactions between cations and the negatively charged backbone phosphate groups. DNA condensation can occur when about 90% of its charge is neutralized by multivalent cations. Early studies have shown that a cation valence of +3 or higher is required to reach this threshold under typical conditions [4]. When the

charge neutralization threshold is reached, the short range attractive forces due to counterion fluctuations become significant enough to condense DNA. This process can be thought of as an "electrostatic zipper" where the charges are arranged in a complementary fashion as DNA strands begin to stack on one another (Figure 1.1).

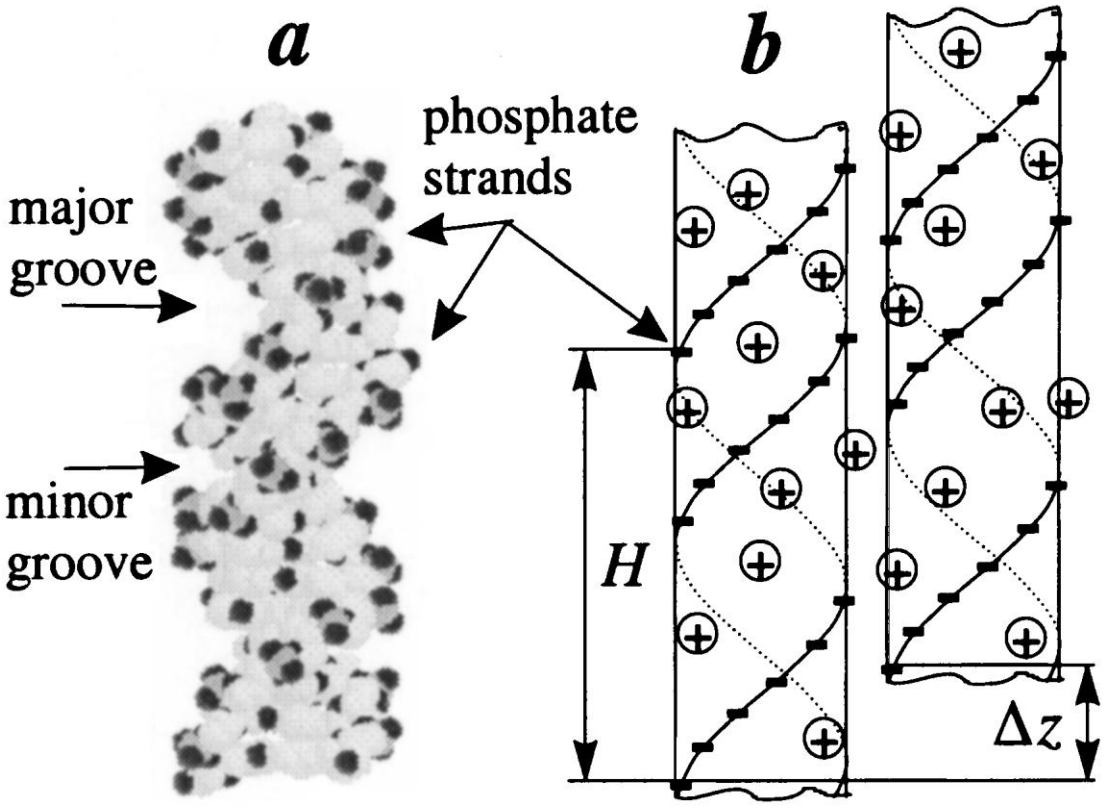

Figure 1.1 Electrostatic zipper motif for DNA condensation
(a) *B*-DNA structure based on crystallographic coordinates. (b) Schematic showing two DNA strands offset from each other such that opposite charges at the points of contact lead to attraction [5]

One of the most striking features of DNA condensation with multivalent cations is the formation of well-defined toroidal or rod-like structures. Evidence from transmission electron microscopy (TEM) shows that toroids have roughly hexagonally packed DNA strands (Figure 1.2). These structures can be formed using a variety of cations such as poly-lysine, spermidine, cobalt hexamine [6]–[8] and

others. Toroidal DNA has also been observed by electron microscopy inside some bacteriophages [9]. Theoretical studies have been carried out to model this behavior of DNA and why certain structures are preferred [10], [11]. The competition of the bending energy and electrostatic attractions lead to the toroidal structures as the most thermodynamically stable. Rods are only slightly less stable, but kinetically favorable and therefore appear quite commonly as well. In the study by Vilfan et al., it was found that the toroid to rod ratio of the population of condensed DNA increased over time, which reinforces this idea [12].

DNA is also often compacted as a complex with larger molecules or proteins. One example is the histone octamer which can interact and bind with DNA via its lysine and arginine groups. Unlike the smaller, multivalent cations, such proteins typically induce bending or wrapping of DNA around the structure. Some synthetic polymer dendrimers and coated inorganic nanoparticles have been designed to mimic such behavior [13]–[15]. Due to their size, they typically do not form rods or toroids when complexed with DNA but rather, may form a beads-on-a-string structure (Figure 1.3) or unorganized globular structures a few hundred nanometers in size.

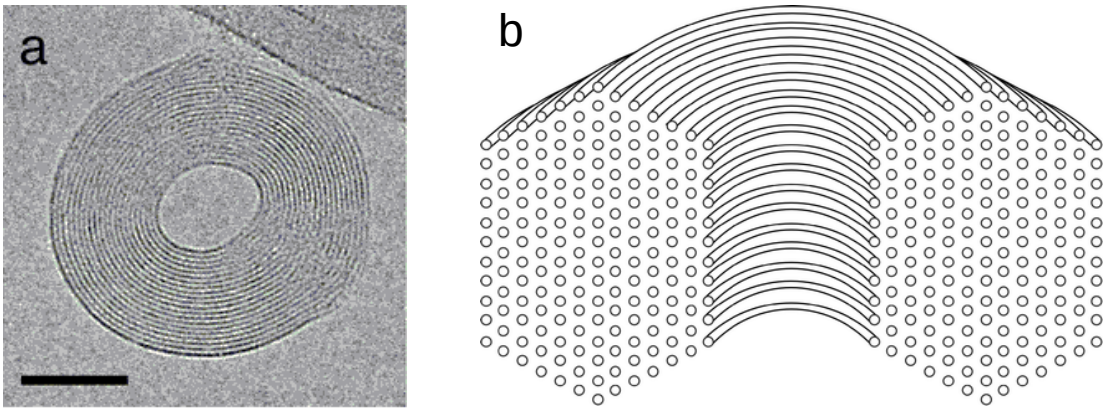

Figure 1.2 DNA toroid structure
(**a**) Top-down view of DNA toroid as seen by TEM with 50 nm scale bar. (**b**) Idealized structure showing perfect hexagonal packing of DNA in the cross section of the toroid [16].

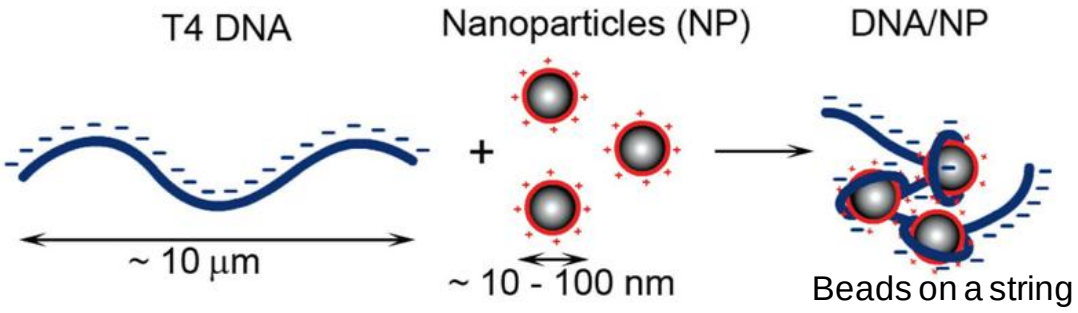

Figure 1.3 DNA-cationic NP interactions
Schematic showing how DNA can interact with cationic nanoparticles, bending and/or wrapping around the particles forming a beads-on-a-string type of structure akin to DNA-histone systems [13].

1.2 Gene therapy and current obstacles

Gene therapy, through the introduction of foreign genetic material can be used to modulate the behavior of a target cell. It has been regarded as a promising technique for the treatment of diseases including hereditary conditions and cancers [17], [18]. One of the main challenges is the engineering of safe, yet efficient gene delivery vehicles. Over the past two decades, the majority of clinical trials have involved the use of modified viruses for gene delivery (Figure 1.4). However, while

viral vectors have been shown to be fairly efficient delivery agents, they suffer from some important limitations including immunogenicity and production difficulties [19], [20]. Synthetic, non-viral gene vectors have thus gained a lot of attention due to their potential to solve these issues, especially the safety concern tied to viral vectors. Such non-viral vectors include cationic polymers, peptides, lipids, and inorganic nanoparticles which although biocompatible, currently struggle to reach the levels of *in vivo* transfection efficiencies of viral vectors [18].

There are a multitude of barriers at both the extracellular and intracellular level involved in the delivery process of DNA. The extracellular level consists of intercellular and intravascular spaces, both of which contain endonucleases that may degrade the therapeutic gene. For this reason, it is important that the genetic cargo be protected which can be achieved by packing the DNA into a nano-sized carrier that is physically and chemically stable. For example, polyplexes are formed when DNA is condensed by cationic polymers. This, in turn, has been shown to greatly reduce the exposure of the DNA to nucleases and therefore increase circulation times [18]. Colloidal stability of the carriers is another important factor to consider as the physiological salt concentrations may screen out the electrostatic repulsions between polyplexes and thus lead to aggregation. Furthermore, interaction with serum proteins and erythrocytes in the blood may also induce aggregation of the complex and lead to rapid clearance by macrophages [21].

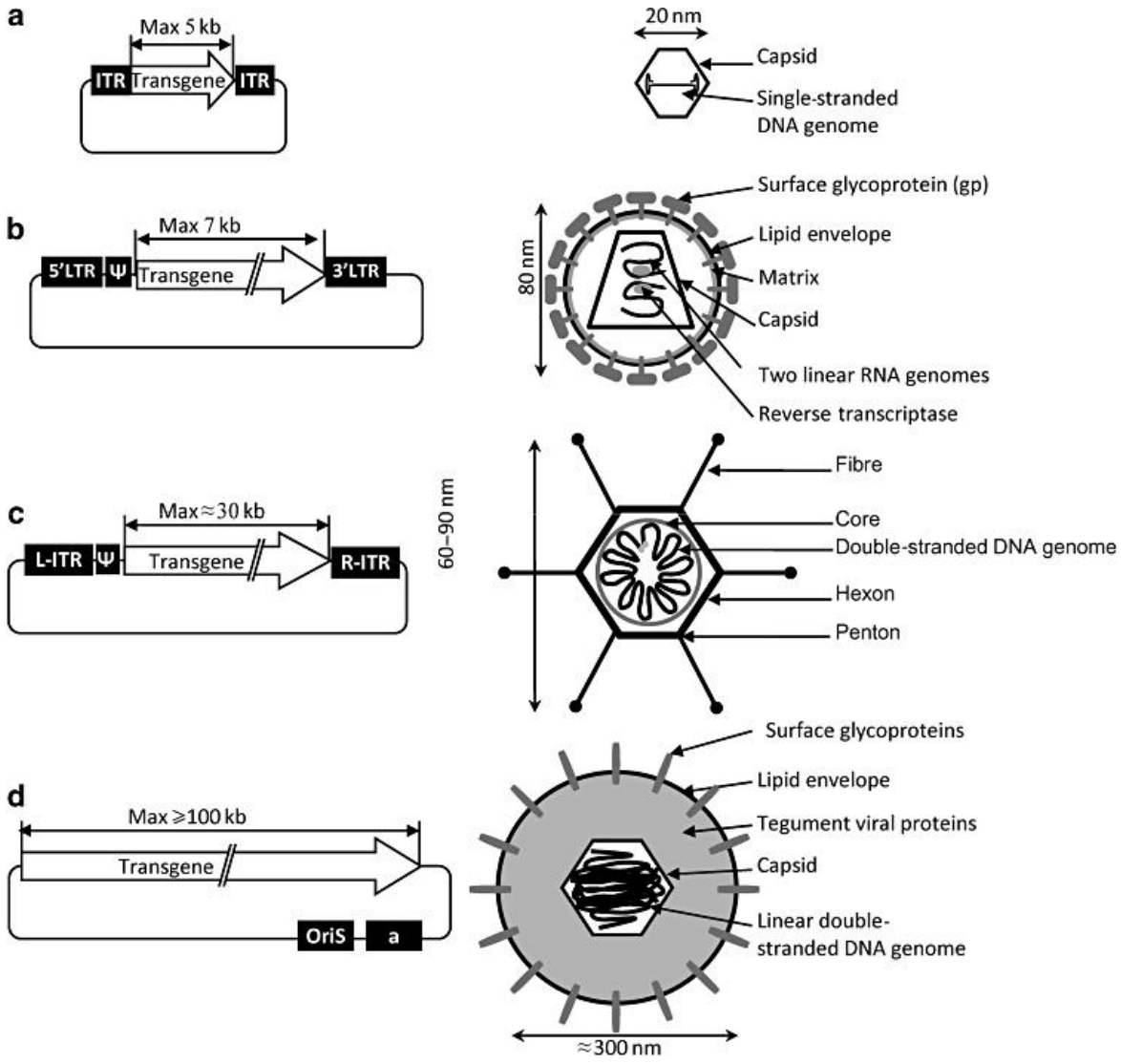

Figure 1.4 The four main types of viral vectors for gene delivery
(**a**) Recombinant adeno-associated virus vector. (**b**) Retroviral vector. (**c**) Gutless adenoviral vector. (**d**) Amplicon vector. [20]

In order for the genetic cargo to reach its target, the DNA complex must be able to bind to the cell surface to initiate endocytosis. Because of the negative charge on the cell surface due to the phospholipid groups, negatively charged DNA is unlikely to associate with the cell surface on its own. Therefore, it is generally necessary to design carriers such that the overall charge of the DNA complex is

positive and condensation of DNA with cationic agents can achieve this. Once internalized however, the gene carrier is enveloped in an endosome. There are two possible fates for an early stage endosome; one is the recycling endosome which returns internalized material back to the cell surface and expels it . The second one is the sorting endosome which redistributes the material within the cell [22]. There is currently little known about the mechanisms which decide the endosome types and whether there is any tendency for gene delivery vehicles to end up in one type or the other. Also, if the DNA remains in the endosomal compartment, it will eventually be degraded by enzymes.

The endosomal stage of the gene delivery process has generally been viewed as a major transfection rate limiting step. There are, however, some mechanisms of endosomal escape which can vary depending on the design of the vector. One such mechanism is through the disruption of the lipid bilayer of the edosome. Delivery agents using cationic lipids can cause such disruptions via the mixing of the cationic lipids with the anionic lipid bilayer of the endosomal compartment [23]. A more common escape mechanism that researches try to exploit is the proton sponge effect [24]. The acidic environment of the endosome can lead to the protonation of gene carriers with pKa values in the acidic range. The influx of protons which also comes along with more water and anions, leads to swelling and eventual bursting of the endosome.

Localization of the DNA to the nucleus of the cell is also necessary in order to access the transcriptional machinery. At some stage however, the DNA must be unpacked from the carrier in order to achieve gene expression. While protection of

the genetic cargo is important for much of the delivery process, the ability to release DNA is a seemingly contradictary, yet crucial property of the carrier [25]. In the case of lipid-based vectors, the fusion of the lipid with the endosomal membrane as mentioned earlier, may also facilitate DNA release [23]. However, there is some evidence that DNA may still require protection while in the cytoplasm, prior to localization on the nucleus [26]. Other studies have shown polyplexes reaching the nucleus intact, but cited slow DNA unpacking as an explanation for low transfection efficiencies [27].

1.3 Cationic Polymers

Polymeric DNA vectors provide many engineering choices given their vast chemical diversity and capability to be functionalized. One of the first such polymers to be studied for gene therapy was poly-L-lysine (PLL), a homopolypeptide of the basic amino acid lysine (Figure 1.5a). While PLL serves as a good DNA condensing agent, studies have shown that it suffers from poor transfection efficiency as well as some cytotoxicity [17], [28]. This is believed to be due to its limited buffering capability and therefore has trouble escaping endosomal vesicles.

Polyethylenimine (PEI) has been one of the most studied and generally considered the standard for non-viral gene delivery. With its high density of amine groups (Figure 1.5b), PEI can condense DNA and possesses a very high charge density at lower pH values. Approximately 15 - 20% of the amines are protonated at physiological pH , thus PEI has a high buffering capacity which is believed to play a role in its effectiveness as a transfection agent. PEI polyplexes, however, have been

found to induce substantial levels of cell death rates [29], [30]. It has been shown, though, that transfection efficiency and cytotoxicity can vary significantly based on structure as well as modifications. Namely, PEI of various molecular weights as well as degrees of branching have been studied [31], [32]. Others have modified PEI by adding polyethylene glycol (PEG) and reported increased stability and biocompatibility [33].

Histidine-lysine (HK) peptides have more recently shown some promise as a non-viral transfection agent [34]–[36]. The idea behind such peptides is that the lysine groups can condense DNA and form stable nanoplexes in physiological conditions. Meanwhile, the histidine groups which have a pKa ~ 6, provide additional buffering capacity while in the low pH environment of an endosome. Through solid-phase synthesis of HK peptides, the amino acid sequence can be carefully controlled allowing insight to how certain HK peptides can be more effective as delivery agents. Furthermore, it has been found that branched HK polymers are more effective carriers relative to linear HK peptides which require liposomes as co-carriers of the plasmids [35]. One of the more successful variants was a four-branched HK polymer with an -HHK- repeating unit (H2K4b) (Figure 1.5c) which was shown to be an effective plasmid carrier *in vivo* [36].

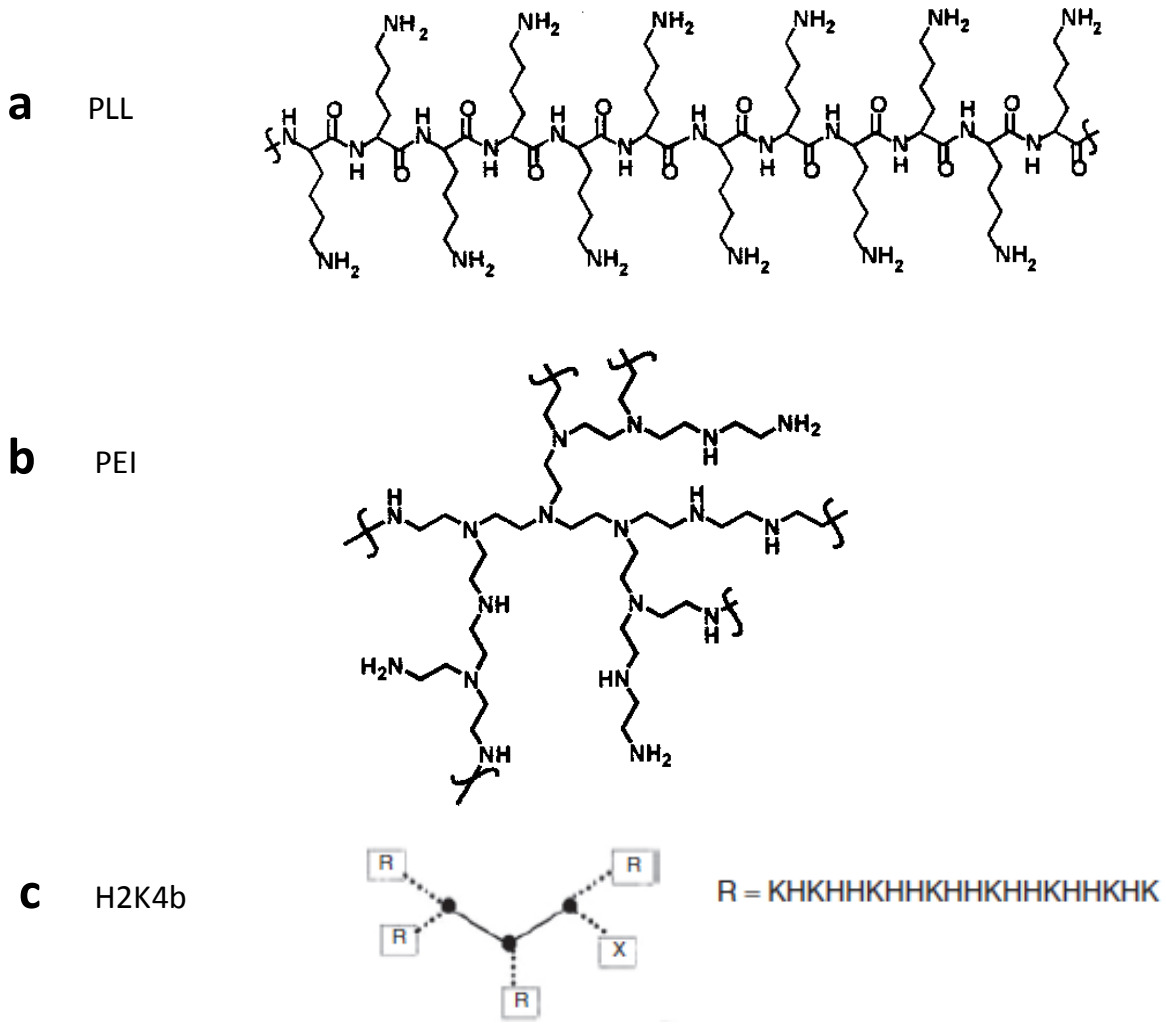

Figure 1.5 Structures of some cationic agents for gene delivery
(a) Poly-L-lysine (PLL). (b) Polyethylenimine (PEI) [37]. (c) Four branched histidine (H)- lysine (K) peptide with three lysine core. "X" represents C-terminal amide group of the lysine core [38].

1.4 Functionalized gold nanoparticles

An alternative class of non-viral vectors make use of a nano-sized inorganic core which can be readily functionalized. Gold nanoparticles (AuNP) are particularly attractive due to them being bioinert, easily synthesized and functionalizable [15]. By introducing a monolayer of cationic ligands on the surface of the gold nanoparticles,

they can bind to plasmids or siRNA and serve as carriers . The resulting structure of such functionalized AuNPs resemble a high molecular weight dendritic polymer with the gold core serving as a space filling element in the center. It has been hypothesized that the use of an inorganic core may reduce the toxicity of the carrier by eliminating exposable functionalities that are normally hidden during complexation [39].

In one study, 2 nm gold nanoparticles were functionalized with various cationic ligands (Figure 1.6) and found that the NPs with first generation lysine dendrons were 28-fold more efficient than PLL on its own for *in vitro* transfection while showing no cytotoxicity [40]. The overall diameter of these modified AuNPs is ~ 6 nm, similar to the size of a histone octamer. Also, the gold-thiolate binding of the ligands has the advantage of being degradable via intracellular glutathione levels. This provides the AuNP carriers a mechanism by which they can release their genetic cargo once inside the cell. In a related study, the AuNPs were functionalized with zero, first, and second generation triethylenetetramine (TETA) $[CH_2NHCH_2CH_2NH_2]_2$ ligands and used for siRNA delivery. The zero and first generations however, were unable to completely bind siRNA before precipitating thus limiting their use. The second generation TETA NP proved to be more stable, presumably due to its higher charge density, while serving as an efficient carrier with minimal toxicity [41].

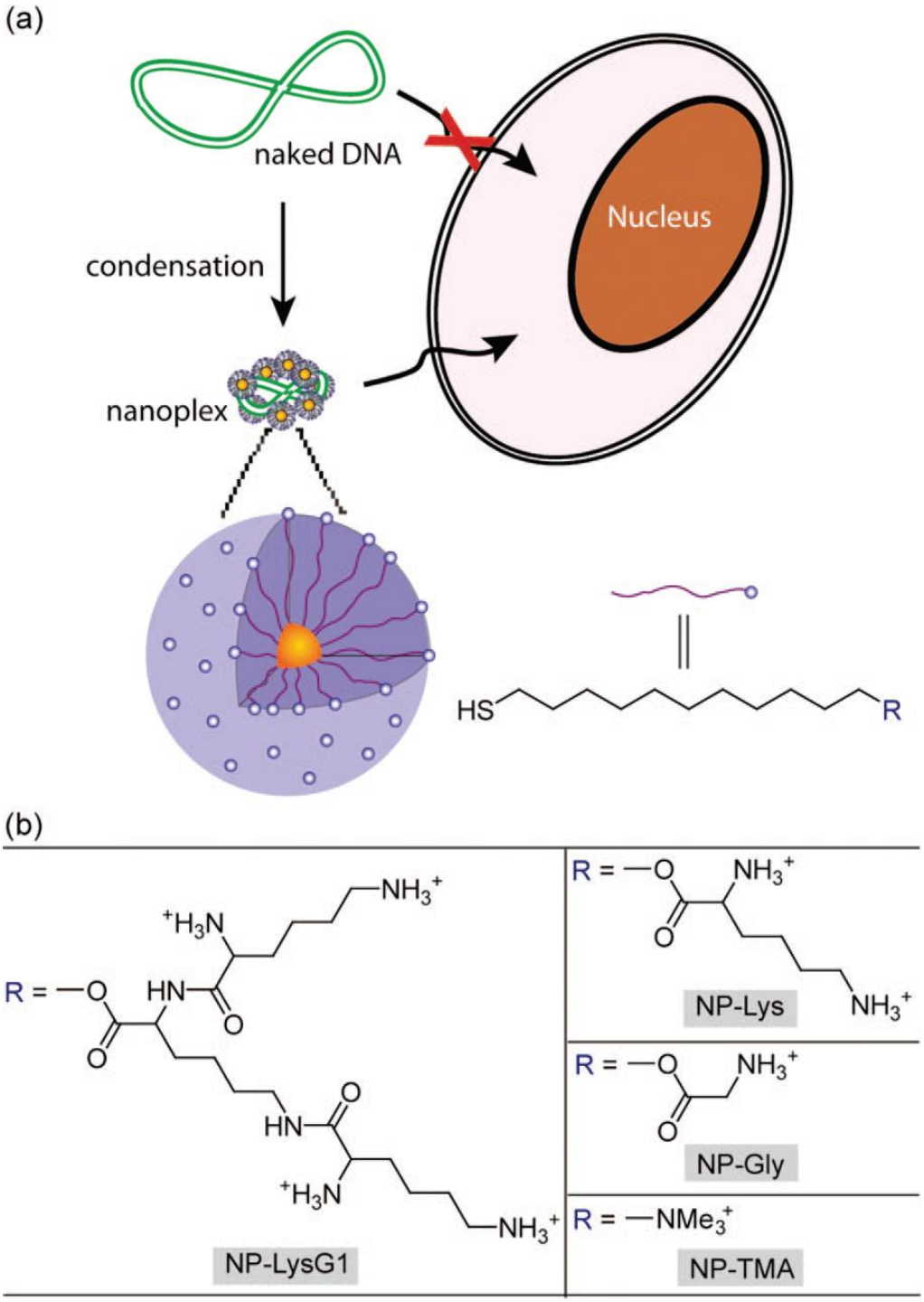

Figure 1.6 Functionalized gold nanoparticles
(**a**) Schematic of coated gold nanoparticle used as gene delivery agent. (**b**) Chemical structure of the head groups on the surface of the nanoparticles. Lys = lysine, Gly = glycine, TMA = trimethyl ammonium [40].

1.5 Role of physical properties of DNA complexes

The relationship between the transfection behaviors and the physical properties of the gene delivery agents remains unclear. Even the optimal size and geometry of the complexes for transfection remains debatable. Generally, smaller particles are more prone to cellular uptake with one study claiming the optimal nanoparticle size for endocytosis to be about 25 - 30 nm [42]. In a study by Prabha et al., poly (D,L-lactide-co-glycolide) (PLGA) complexes were separated by size using a membrane with 100 nm sized pores [43]. The smaller particles (mean diameter ~ 70 nm) showed much higher transfection efficiencies than the larger particles (mean diameter ~ 200 nm). However, their surface charge, cellular uptake and DNA release were similar for both fractions, suggesting other unknown mechanisms may be playing a role. Others have failed to observe any correlations between the physical properties (size, charge, and shape) of the complexes and their transfection activity [44], [45].

DNA complexes prepared by vortexing generally tend to form a heterogeneous distribution of nanoparticles and exhibit some degree of aggregation [46]. This can complicate matters when attempting to elucidate the structure-function relationship of a gene delivery system. It is therefore of great interest to employ a variety of characterization techniques in order to probe all species of complexes, and/or reduce the heterogeneity in complex formation. Atomic force microscopy (AFM) is a well known technique often used to characterize such systems. AFM allows great resolution of nano-sized particles which can give structural insights at the molecular level. While many researchers choose to dry down their systems prior

to AFM imaging, it is also possible to image the samples in fluid. Imaging in fluid avoids the possible artifacts and structural changes that may arise from drying down organic materials. The mica that serves as a substrate for AFM imaging can also give us another level of control over the observation and formation of the DNA complexes. Here, we will specifically be characterizing complexes formed with a 25 kDa branched PEI, an HK peptide with four branches, and functionalized gold nanoparticles. Dynamic light scattering (DLS) will also be used to compliment the AFM data on the polyplexes with PEI and HK.

Chapter 2: Observation of DNA condensation by functionalized gold nanoparticles using AFM

2.1 Introduction

Gold nanoparticles (AuNPs) can be utilized as a non-viral transfection agent. The gold cores are readily synthesized, nontoxic, and can be functionalized for both diagnostic and therapeutic purposes [47]. Ghosh et. al has shown the potential of AuNP systems for DNA delivery using AuNPs functionalized with lysine dendrons [48]. The gold core diameter was ~ 2 nm, with a final diameter of ~ 6 nm after addition of the amino acids, roughly resembling the histone octamer in terms of size and surface functionality. It was found that the nanoparticles with the highest ammonium group density, which in this case was the first generation lysine dendrons with about 320 amine groups per nanoparticle, provided the best compaction of DNA as well as delivery efficiency. Furthermore, the gold-thiolate binding of the ligands to the gold core provide a mechanism by which the DNA can be released via manipulation of glutathione levels in the cells.

AuNPs functionalized with triethylenetetramine (TETA) of various generations (G0, G1, and G2) were studied for siRNA delivery by Kim et. al [41]. Only the G2 AuNP was able to bind with all the free siRNA without leading to precipitation. This shows the importance of tuning the surface charge density of the AuNPs. The G2 TETA nanoparticles were then shown to be efficient for siRNA delivery with high knockdown efficiency and no cytotoxicity.

This work will investigate the physical characteristics of AuNPs functionalized with TETA, complexed with DNA using AFM. A variety of conditions will be used including varying relative concentrations, salt levels, and sample preparation techniques to probe the complex formation process from multiple angles. The aim of this study is to elucidate the connection between the observed characteristics of the complex morphologies and formation behavior, to their viability as transfection agents based on previous studies, and compare them.

2.2 Materials and Methods

2.2.1 Materials

Gold nanoparticles (AuNPs) with a diameter of 2 nm were synthesized and functionalized via a ligand exchange reaction by Dr. Rotello's group [39]. The thiol connects the gold core with the triethylenetetramine (TETA) (Figure 2.1). The AuNPs are first prepared as monolayer-protected clusters (MPCs) using the Brust-Schiffrin reaction. In this method, $AuCl_4^-$ is mixed with the surfactant tetraoctylammonium (TOAB) followed by reduction using sodium borohydride ($NaBH_4$) in the presence of alkanethiols. The MPC's are then further functionalized with TETA ligands via a place exchange reaction to replace the head group. There are about 80 ligands per nanoparticle. The generation 2 (G2) TETA NPs has four branches per thiol. 1/2 λ DNA (24kbp) (Sigma Aldrich) was used for the bulk mixing experiments in section 2.3.1 while tdTomato plasmid (5.4 kbp) was used for the other experiments.

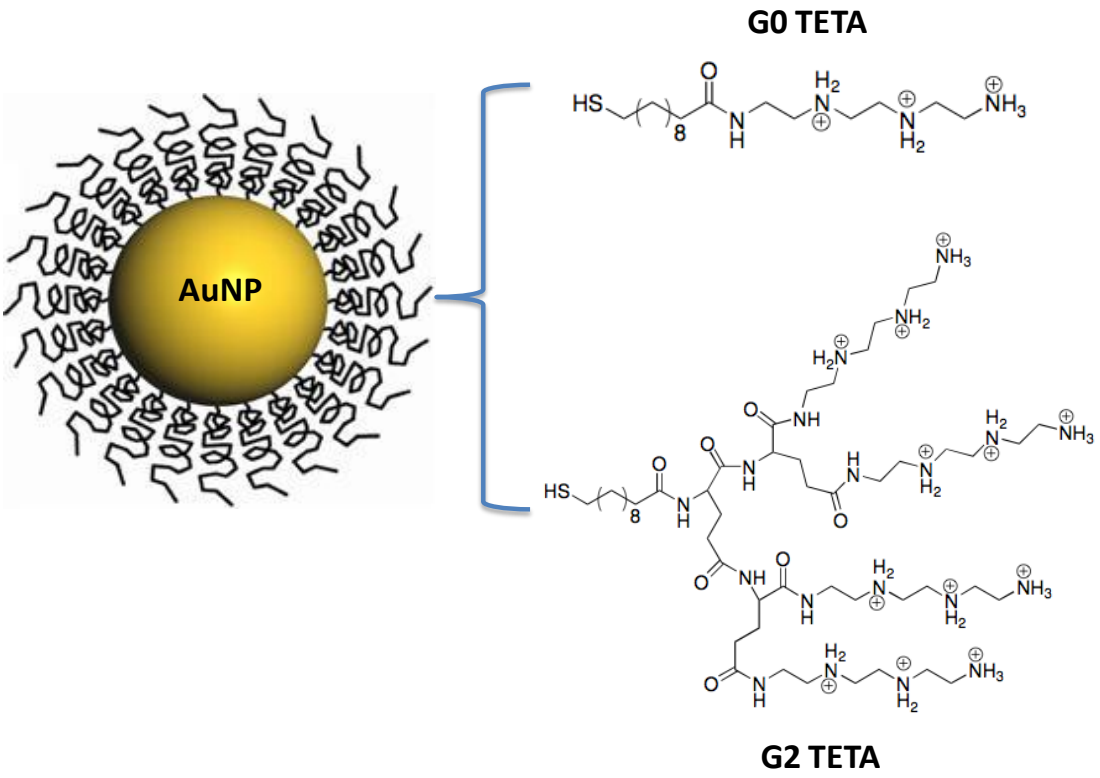

Figure 2.1 Gold Nanoparticle and ligand chemical structure
Schematic of AuNP with solid 2 nm gold core coated with a monolayer of ligands for a total NP size of ~ 6 nm. The chemical structures of the two ligands (G0 and G2 TETA) that were used are shown on the right.

2.2.2 AFM

Atomic force microscopy (AFM) is a well established method for imaging the topography of a sample down to the nanoscale. Unlike electron microscopy techniques, AFM does not suffer from poor contrast when imaging organic materials due to their low atomic numbers. Furthermore, AFM samples can readily be measured while in fluid and therefore preserve their hydrated state. The AFM used here is an Asylum MFP-3D (Oxford Instruments) (Figure 2.2). It uses an 860 nm superluminescent diode (SLD) which is focused near the head of the cantilever which is then reflected onto a mirror and collected on a position-sensitive diode (PSD).

Both vertical and lateral (twisting) movements of the cantilever are tracked by the light spot on the PSD.

In contact mode imaging, the topography is mapped out by raster scanning with the cantilever on the sample surface while maintaining a constant deflection (normal force) which can be specified by the user. When the tip comes across a surface feature, its deflection will change which is detected by the PSD. The feedback will then readjust the height position of the cantilever via the Z-piezo. Movements due to the Z-piezo is tracked and mapped out during the scanning process to obtain the topographical (height) data.

Tapping or A/C mode is also frequently used which is a similar concept but instead of maintaining constant deflection, the cantilever oscillates above the sample surface and the amplitude is maintained by the feedback loop. For the MFP-3D, the cantilever is acoustically driven by a shake piezo at a user defined amplitude and frequency. As the oscillating tip approaches the sample surface, the amplitude is dampened. A set point amplitude of 80 - 90% of the free amplitude is typically used to sufficiently engage and "tap" the surface. Surface features will lead to different degrees of dampening during the scan which is compensated accordingly by the Z-piezo to maintain the set point amplitude. As well as getting height data, tapping mode can track phase shifts of the oscillating cantilever as it scans the surface. Phase shifts are sensitive to the properties of the material that is being scanned, so even when there is little to no height difference, scanning over areas with differing materials may be more clearly revealed by the phase data. Furthermore, tapping

mode applies less force on the sample which is ideal when imaging soft materials as contact mode can often be disruptive.

Unless otherwise stated, images were obtained using tapping mode with a set point of about 85 - 90%. Most images were taken at a scan rate of 2 Hz with 256 points and lines. MLCT or MSNL (Bruker) D cantilevers were used. These cantilevers are silicon nitride with a typical resonance frequency of about 9 kHz when used in fluid, and spring constant of approximately 0.03 N/m according to manufacturer specifications. The MLCT cantilevers also have SiN tips with nominal radii of about 20 nm while the MSNL have Si tips which could go down to 2 nm allowing for better resolution. Images were obtained and flattened using the Igor (WaveMetrics) software.

Figure 2.2 Asylum MFP-3D
Photo of the MFP-3D AFM head resting over the sample stage. The setup rests on top of a floating table for mechanical isolation and kept inside an insulating box.

2.2.3 AFM sample preparation

For the bulk-mixing experiments, ½ λ DNA was diluted to 1 ng/μL in 10 mM HEPES buffer with 10 mM Ni^{2+} . The G0 NPs were diluted to 0.5 μM in 10 mM HEPES buffer. 1 μL of the G0 NP solution was added at a time to 10 μL of the DNA solution while gently tapping and incubated for ~2 min. This was repeated until the desired amount of NPs were added. 10 μL of the complex solution was then dropped on freshly cleaved mica and washed with filtered DI water. The imaging was done immediately after in liquid. Heights were analyzed using ImageJ software to find the maxima of the spherical, DNA-NP aggregate regions.

For the surface complex formation experiments, 10 μL of 0.5 ng/ μL DNA in 1 mM $NiCl_2$, 2 mM Mg, 10 mM HEPES (pH 7.4) buffer incubated on freshly cleaved mica prior to adding 10 μL of 0.4 μM G2 NPs in same buffer. Afterwards, 1 μL 0.1 M NaOH was added to the imaging solution (80 μL of buffer) then washed with 10 mM $NiCl_2$, 10 mM HEPES after 10 minutes to improve the image quality of the DNA.

2.3 Results and Discussion

2.3.1 Bulk mixing of G0 NPs and DNA

G0 NPs and 1/2 λ DNA were combined together in solution at various ratios prior to depositing on mica for AFM imaging. At the two lower N/P ratios (N/P = 8 and 16), we can see the binding of the AuNPs to DNA, usually clustering around the center of the DNA molecules (Figure 2.3a-b). The DNA strands that protrude from the central, condensed structure often loop back into the center resulting in a flower-like morphology for the DNA-NP complex. As the G0 NP to DNA ratio is increased,

the central clusters continue to grow in size. The average heights of these clusters as measured by AFM increase from ~ 20 nm to over 100 nm while also having a broad distribution, with a standard deviation of 83 nm at the highest N/P ratio (Figure 2.3d). Phase mode imaging from the AFM of some of the larger complexes can more clearly show their granular structure (Figure 2.4). In an attempt to get a better understanding of the organization of these complexes, we repeatedly scanned the complexes with various force levels from the tip. This proved difficult to control precisely, often unintentionally dragging parts of the complex due to the significant forces from tapping mode [49] or simply sweeping the entire complex aside from the higher forces of contact mode. Nevertheless, images were obtained that showed DNA strands with attached NPs protruding from the large cluster along the AFM tip scanning direction (Figure 2.4b). This suggests that the NPs initially bind along the DNA in random locations in a beads-on-a-string fashion, followed by aggregation of the NPs causing parts of the DNA strand to fold back into the central cluster forming the observed flower-like morphology of the complex. The large heterogeneity of these complexes, however, may make it difficult to properly analyze and draw connections between the physical properties of the complex and its likely efficiency in transfection experiments. It is therefore desirable to try other methods of complex preparation to better control the condensation process of the DNA with these NPs.

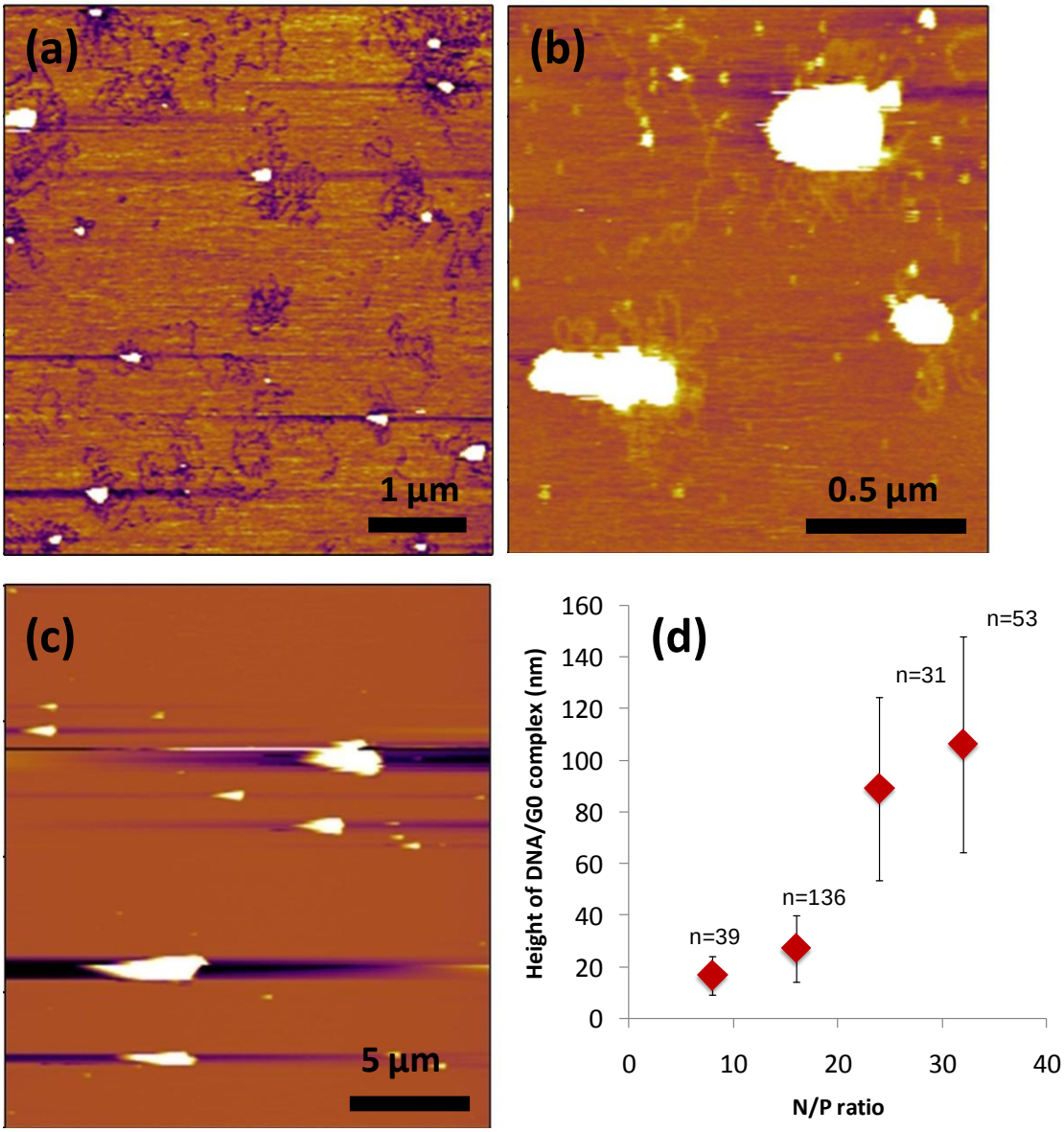

Figure 2.3 Progression of DNA condensation with G0 NPs by bulk mixing
AFM images of ½ λ DNA complexed with G0 NPs by bulk mixing method after adding 4 µL (N/P ~ 8) (**a**), 6 µL (N/P ~ 16) (**b**), and 8 µL (N/P ~ 24) (**c**) of 0.5 µM G0 NP solution into 10 µL of DNA solution. DNA-mediated aggregation of NPs results in the formation of clusters of NPs on the DNA. As N/P ratio is increased, more nuclei of NPs form and grow in size, forming flower-like structures with the NP cluster in the center with a DNA corona. Heights of complexes as measured by AFM are plotted in (**d**).

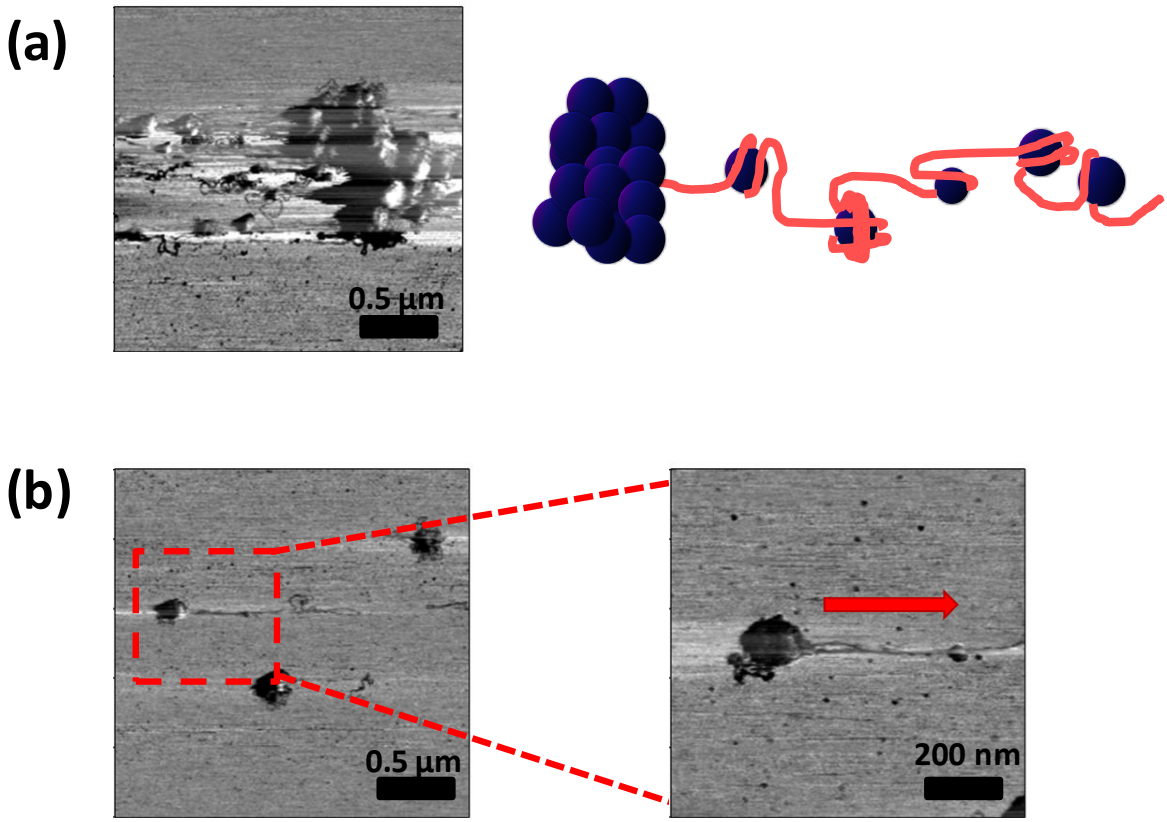

Figure 2.4 Mechanical disruption of G0 NP complexes with AFM
DNA/G0 complexes prepared by mixing DNA with G0 NPs at N/P = 24 in solution. Granular structure is seen in AFM phase image with DNA and NPs protruding from the main cluster (**a**). Mechanical force from the AFM tip can often pull out DNA with NPs attached in a beads on a string manner, along the direction of the tip movement (red arrow) (**b**).

2.3.2 DNA-NP interactions on mica surface

In order to have a better sense of the complex formation process and to possibly improve homogeneity of the complexes, DNA and NPs were each adsorbed onto the mica surface in separate steps rather than being mixed together in solution. NP-decorated plasmid DNA can be seen when G0 NPs are first adsorbed onto the mica followed by addition of the DNA solution (Figure 2.5a). Kinks and sudden changes in direction of the DNA strands at the locations of the NPs were common,

probably due to some bending or wrapping of the DNA around the NPs. While the DNA is able to bind to the NPs on the mica, there were no condensed structures observed. This remained to be the case regardless of how many G0 NPs were initially added onto the mica surface. Unlike how NP-DNA behaves in solution, the strong NP-mica surface interaction prevents the NPs from forming a cluster and forming a condensed complex. To help weaken the NP-mica interaction and promote more mobility, NaCl concentrations in the buffer were increased (Figure 2.5b-c) to provide greater electrostatic screening. Despite this, however, DNA failed to condense into more compact structures and the same morphologies were observed. Interestingly though, a significantly greater number of DNA molecules were adsorbed at intermediate NaCl concentrations (~ 50 mM NaCl). This may be due to the enhanced ability of DNA to wrap the NPs at moderate NaCl concentrations due to electrostatic screening of phosphate charges on the DNA backbone, leading to increased DNA flexibility [13], [50], [51] and therefore more stable DNA-NP complexation. If NaCl concentration is further increased however, the electrostatic screening may simply prevent the NPs from binding onto the DNA at all.

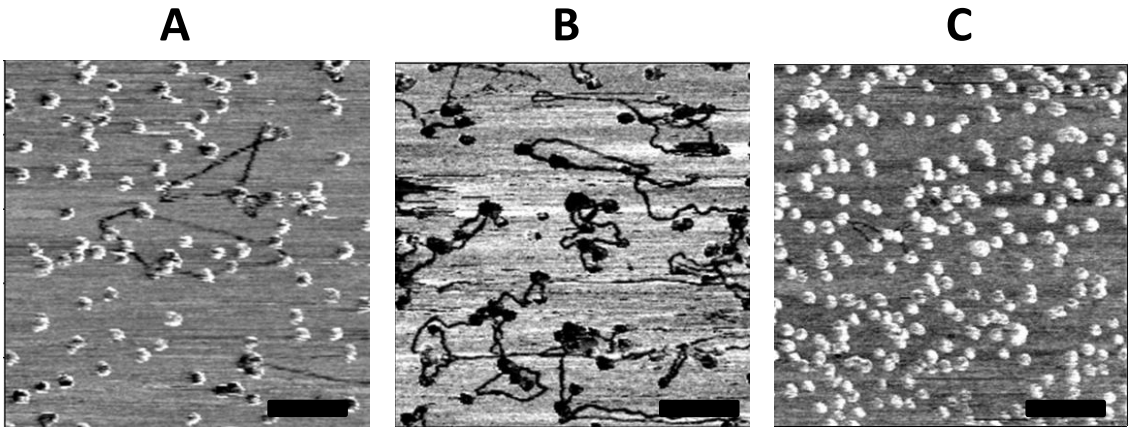

Figure 2.5 Effect of NaCl on G0/DNA complexation
A 10 μL droplet of 0.25 μM G0 NPs was incubated on the mica prior to washing and adding 10 μg/mL DNA in 10 mM HEPES buffer (**a**), with 50 mM NaCl (**b**), and 100 mM NaCl (**c**). The intermediate NaCl concentration showed the highest density of DNA on the mica surface while 100 mM NaCl showed the least. All showed a similar beads on a string morphology. Scale bar is 200 nm.

Another approach we used to promote interactions favorable for DNA condensation on the mica surface was by adding NaOH into the droplet after adding both DNA followed by the G0 NPs onto the mica. When G2 NPs are added after adsorbing on the mica surface, we see the uncondensed beads on a string morphology (Figure 2.6a). After adding 1 μL of 0.1 M NaOH then washing with a HEPES buffer with 10 mM $NiCl_2$, the complexes appeared more compact, with clustering of the NPs and flower-like morphologies (Figure 2.6b-c). These morphologies appear to be an intermediate stage between the fully uncondensed DNA and the globular aggregates seen when the NPs and DNA are simply mixed in solution as seen in Figure 2.6d. The exact mechanism(s) which drives this behavior is still unclear. The amount of NaOH added into the solution for these observations is not enough to significantly shift the pH of the solution with the buffer. We therefore postulate that the addition of NaOH may affect the interactions between the HEPES molecules and the DNA

and/or NPs. There is evidence that the two positive charges of the HEPES can interact quite strongly with the phosphates on the DNA, helping it adsorb more strongly to the mica relative to other buffers such as Tris [52]. The addition of NaOH may help to weaken the interactions between the DNA and HEPES, which then temporarily releases the DNA allowing some mobility from the mica surface.

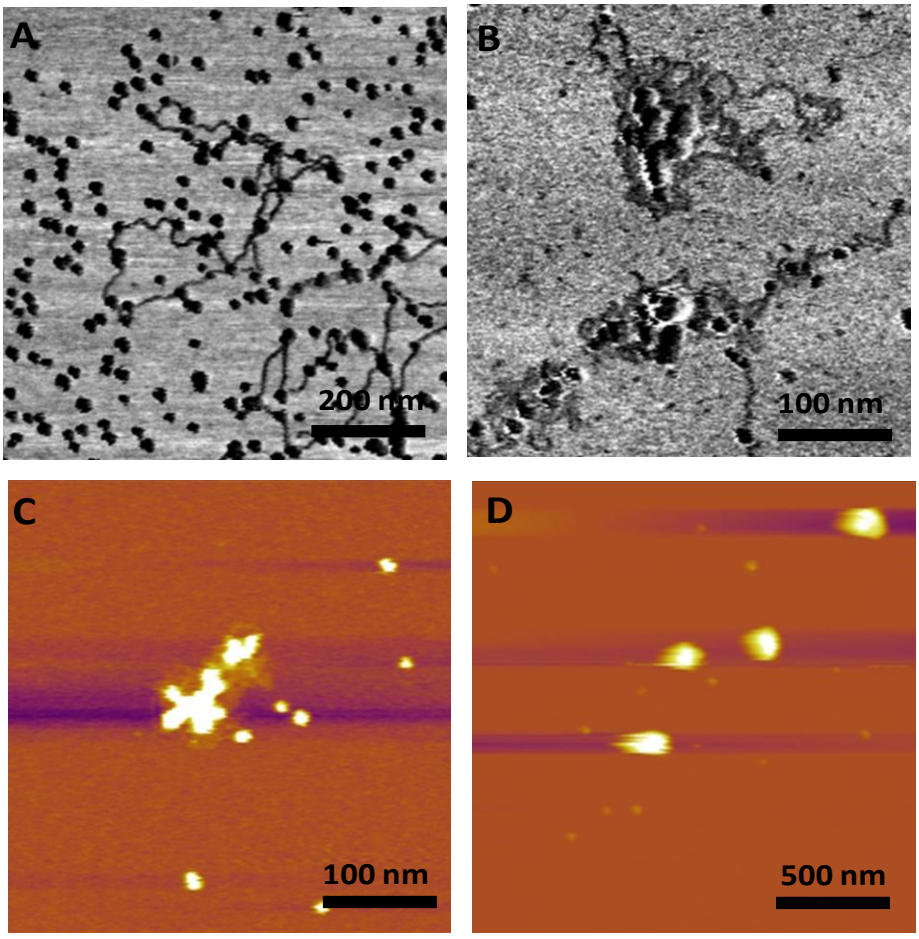

Figure 2.6 DNA condensation with G2 NPs on mica surface
(**a**)10 μL of 0.5 ng/ μL DNA in 1 mM $NiCl_2$, 2 mM Mg, 10 mM HEPES (pH 7.4) buffer incubated on freshly cleaved mica prior to adding 10 μL of 0.4 μM G2 NPs in same buffer. (**b**-**c**) Same procedure with the addition of 1 μL 0.1 M NaOH to imaging solution (80 μL of buffer) then washed with 10 mM $NiCl_2$, 10 mM HEPES after 10 minutes to improve image quality of DNA. (**d**) Same amount of DNA and G2 NPs but mixed and incubated in buffer solution for 30 min prior to dropping on mica. Complexes in (**d**) were typically 30-40 nm in height and ~ 100 nm in width.

2.4 Conclusions

Through various sample preparation techniques we have observed multiple stages in the DNA-NP complexation process. By either fixing the DNA molecules or the NPs on the mica surface, NPs can bind to the DNA resulting in a beads-on-a-string morphology akin to DNA-histones system. Sudden directional changes along the DNA strand at the points of contact with NPs suggests the bending or wrapping of the DNA around the NPs. Addition of NaOH into G2 NP-DNA system adsorbed on the mica surface resulted in enhanced mobility and aggregation of the NPs in the DNA complex. Some of these complexes resembled the flower-like morphologies seen when the DNA and NPs were incubated together in solution. When a DNA complex is fully saturated with NPs, the complexes assume more globular morphologies with a granular appearance. Finally, mechanical manipulation of the complexes revealed some of the internal structuring of these fully saturated NP-DNA complexes, showing that the beads-on-a-string morphology is likely the primary structure of these complexes.

Chapter 3: DNA condensation with PEI

3.1 Introduction

Polyethyleneimine (PEI) is well known transfection agent that can be considered one of the standards when it comes to non-viral gene delivery. Many variations of PEI have been studied, including high or low molecular weight PEI, linear or branched PEI, as well as other modifications and hybrid systems. High molecular weight PEI is capable of protecting the entrapped DNA from enzymatic degradation, but induces greater cytotoxicity due to its noncleavable structure [30]. Low molecular weight PEI on the other hand, has been shown to have less cytotoxicity but suffers from low transfection efficiency [53]. A common strategy to help alleviate this issue is to bind low and high molecular weight PEI with biodegradable linkages such as disulfide bonds. The disulfide bonds provide an escape mechanism for the DNA into the cytosol via redox reaction in the presence of the high levels of intracellular glutathione (GSH) [54]. So far though, the general consensus seems to be that it is difficult to achieve high transfection efficiencies with PEI without also having high levels of cytotoxicity, therefore limiting its *in vivo* applications.

Physical characterization on the polyplexes from a previous study on 13.4 kDa linear PEI has shown that the initially formed PEI-DNA complexes begin to aggregate at N/P ~ 2, but form stable complexes at N/P > 10 with diameters of 170 ± 65 nm [55]. It was also shown that at N/P > 2.5, much of the added PEI was not bound to DNA and remained free in solution. It was argued that the free PEI may

contribute to the cytotoxicity often associated with PEI polyplexes, but at the same time play a role in its transfection efficiency. While some of the literature only reports seeing globular structures in the range of a few hundred nanometers, others have observed rod-like or toroidal structures. Toroids, for example, were observed by TEM using 25 kDa PEI to form the polyplexes [56].

Typically, polyplex samples are dried down on the substrate prior to imaging. Our AFM methods will allow the observation of various morphologies of the complexes while they remain in an aqueous environment. The PEI that will be used here is a branched polymer with primary, secondary, and tertiary amines. The polyplex formation will be characterized across a wide range of PEI amines to DNA phosphate (N/P) ratios via AFM as well as DLS and zeta potential measurements. A careful physical characterization of the polyplexes can be crucial to eventually understanding what leads to their transfection behavior, and lead to a more rational design process for future non-viral vectors.

3.2 Materials and Methods

3.2.1 AFM

The plasmid used in these experiments was pBR322 with a length of 4361 bp (New England BioLabs). The plasmid DNA is diluted to 20 mg/L in a 10 mM Tris buffer (pH 7.4) solution. The plasmid solution is then added to a solution of equal volume with appropriately diluted 25 kDa branched PEI (Sigma Aldrich) in 10 mM Tris buffer to obtain the desired N/P ratio. The mixture is gently vortexed for 10 seconds then incubated at room temperature for 30 min. After incubation, 80 μL of

the complex solution is dropped onto a freshly cleaved mica surface or a PEI-coated mica surface.

To coat the mica surface with PEI, a 10 μL droplet of 10 μM PEI is deposited on freshly cleaved mica and incubated for 5 min (Figure 3.1). The coated mica is then rinsed by adding 100 μL of buffer solution, incubating for 1 min, then sucked up by the pipette. This is repeated five more times to ensure there is a negligible amount of excess, unbound PEI present in the solution. The PEI-coated mica surface allows for clear imaging of uncondensed or partially condensed DNA which normally would not adsorb onto the negatively charged mica surface. Furthermore, it was found that this method allows the imaging of rods and toroids which still carry a slight overall negative charge.

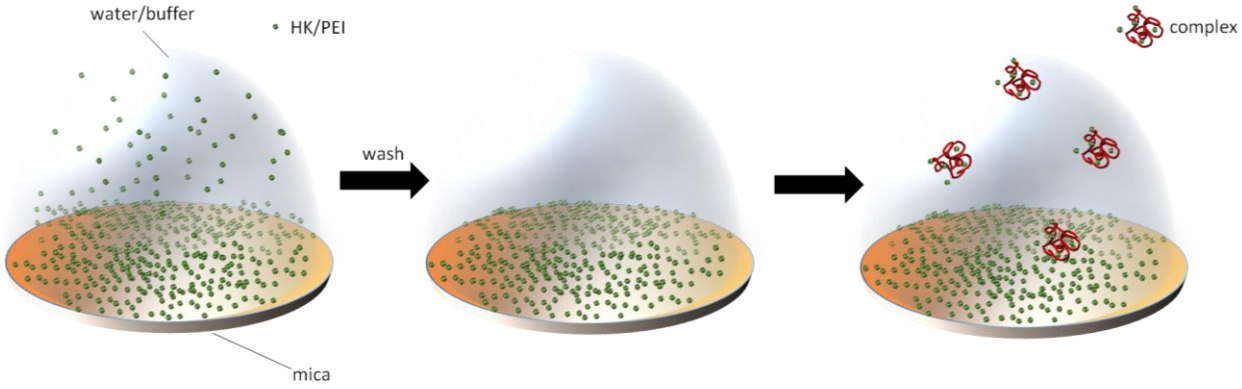

Figure 3.1 AFM sample preparation method
Schematic sample preparation showing the deposition of the condensing agent (PEI) onto the mica, followed by washing to remove the excess PEI before adding the complex solution.

3.2.2 DLS

Dynamic light scattering (DLS) is a technique that measures the Brownian motion of particles which is then used to determine the particle size. The Malvern

Zetasizer ZS90 (Spectris) illuminates the particles with a 633 nm He-Ne laser with a max power output of 4 mW. The scattered light is captured on a detector, forming a speckle pattern which is tracked over time. Fluctuations due to Brownian motion will lead to a decrease in correlation between the current and initial speckle pattern. The rate at which the correlation function decays corresponds to the diffusion coefficient of the particles, which can then be used to determine the hydrodynamic radius using the Stokes-Einstein equation:

$$D = \frac{k_B T}{6\pi\eta r}$$

where *D* is the diffusion coefficient, k_B is the Boltzmann constant, T is temperature, η is the viscosity, and r is the hydrodynamic radius for a spherical particle. The size distribution data is fundamentally based on the scattering intensity. Since larger particles scatter far more (proportional to the sixth power of its diameter), intensity-based distribution data will be skewed towards the larger particles. Using Mie theory, the data can be converted to particle volume which can then be converted to a number distribution. However, small errors in the correlation function fitting can lead to large errors in the number distribution.

Nanoplex solutions for DLS measurements are prepared as in section 3.2.1. 50 μL of the sample is pipetted into a disposable low volume polystyrene cuvette (ZEN0188, Malvern). The sample is then placed in the Zetasizer where it is allowed to equilibrate for 2 min at 25° C. The attenuator setting is manually set to 11 which corresponds to no attenuation, for maximum signal. Three measurements are recorded for each sample, and the number of runs per measurement is set to automatic. All size data reported here is based on the intensity distribution.

3.2.3 Zeta potential

Charged particles in solution will attract counterions forming an electrical double layer (Figure 3.2). The inner layer is known as the Stern layer, where the counterions are more strongly bound while the outer or diffuse layer consists of less tightly bound counterions. Within the diffuse layer is the slipping plane, a boundary where ions beyond it do not move with the particle. The electric potential at this boundary is the zeta potential. Particles carrying a high enough like charge in solution will repel each other, preventing aggregation. Generally, particles with a zeta potential with an absolute value greater than approximately 30 mV are observed to be stable in solution.

The zeta potential can be calculated by measuring the electrophoretic mobility of a particle and applying the Henry equation:

$$U_E = \frac{2\epsilon\, z\, f(Ka)}{3\eta}$$

where U_E is electrophoretic mobility, ϵ is the dielectric constant, z is the zeta potential, η is viscosity, and $f(Ka)$ is Henry's function. For aqueous media with moderate electrolyte concentrations, $f(Ka)$ can be set to 1.5 which is known as the Smoluchowski approximation. Non-aqueous media generally use the Huckel approximation which is 1.0. The electrophoretic mobility can be measured using laser Doppler velocimetry. A potential is applied to the electrodes of the zeta cell which cause charged particles to flow in one direction. A beam scattered by the solution is combined with a reference beam, which results in a fluctuating intensity with the rate of fluctuations depending on the velocity of the particles.

500 uL of the polyplex solution is pipetted into a disposable folded capillary cell (DTS1070, Malvern) after rinsing it with ethanol. The zeta cell is inserted into the Zetasizer and the sample is allowed to equilibrate for 2 min at 25° C. Each sample was measured three times and the number of runs per measurement was determined automatically by the software. The Smoluchowski approximation was used for the Henry's function in all samples.

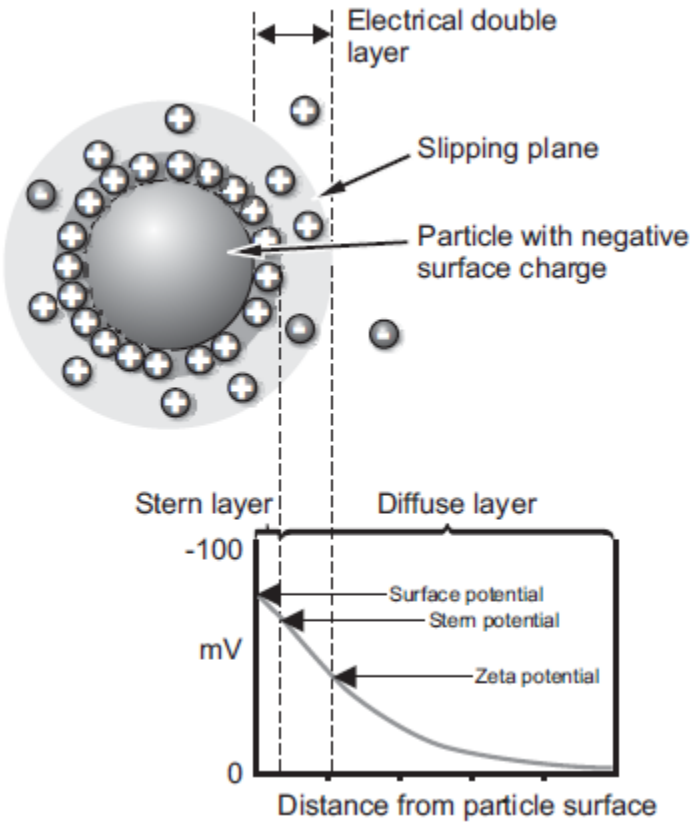

Figure 3.2 Electrical double layer and zeta potential
Schematic showing the two counterion layers surrounding a charged particle: the Stern layer where the ions are tightly bound, and the diffuse layer. Within the diffuse layer lies the slipping plane which is where the zeta potential is defined.

3.3 Results

3.3.1 PEI-DNA complexes observed via AFM

Some condensation of DNA can be observed at N/P ratios as low as 0.05 although the majority of the DNA remained uncondensed (data not shown). As more PEI is added, we see an increase the relative number of condensed morphologies relative to the uncondensed DNA, which included a roughly equal mix of rods, toroids, and globular structures (Figure 3.3 b - d). When the plasmid is added to the PEI-coated mica on its own, we see only uncondensed DNA structures (Figure 3.3a). Therefore, the condensation process of DNA occurs while in solution with PEI, and not because of the PEI on the mica surface which serves to bind the negatively charged species including rods and toroids. Closer inspection of the rods and toroids can be seen in Figure 3.4. The diameters of the toroids (measured from peak to peak in the height trace) are 56 ± 9 nm, with a circumference that coincides well with the length of the rod-like structures which were measured to be 176 ± 52 nm. At N/P ~ 2, most condensates on the PEI-coated mica are globular in appearance (Figure 3.5a). At higher N/P ratios, complexes were no longer observable on PEI-coated mica but instead seen on bare mica. This indicates a transition from polyplexes with a negative surface charge to an overall positive charge. All complexes observed at the higher N/P ratios had globular morphologies (Figure 3.5b) with heights and widths of 20 ± 11 nm, and 86 ± 15 nm, respectively.

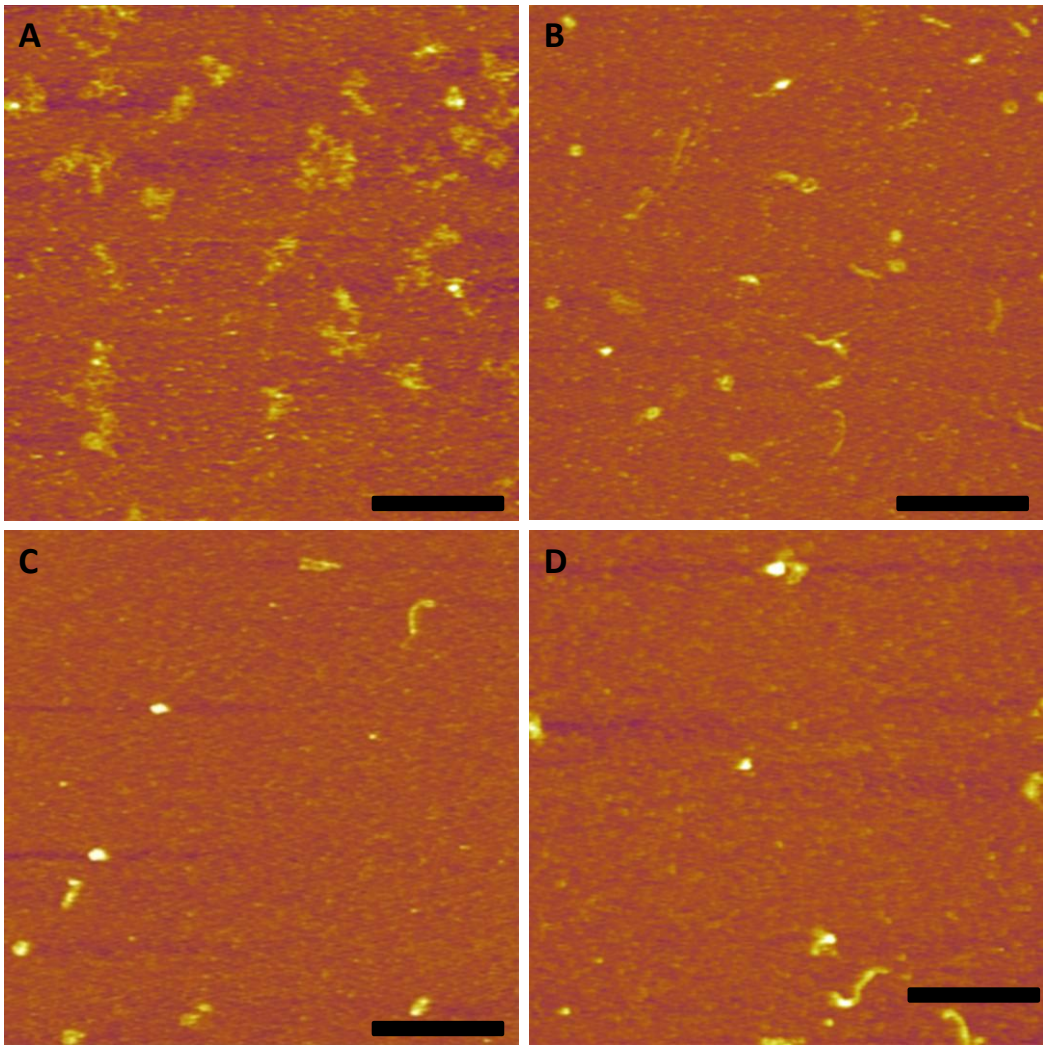

Figure 3.3 AFM images of PEI polyplexes on PEI-coated mica
PEI-DNA complexes were prepared at N/P ratios of 0.2 (**B**), 0.5 (**C**), 1.0 (**D**), and deposited on PEI-coated mica. No condensed structures are seen when only the DNA solution on its own is deposited on the PEI-coated mica surface (**A**). The morphologies of the condensed polyplexes consists of a mixture of rods, toroids, and globular structures. Scale bar is 500 nm.

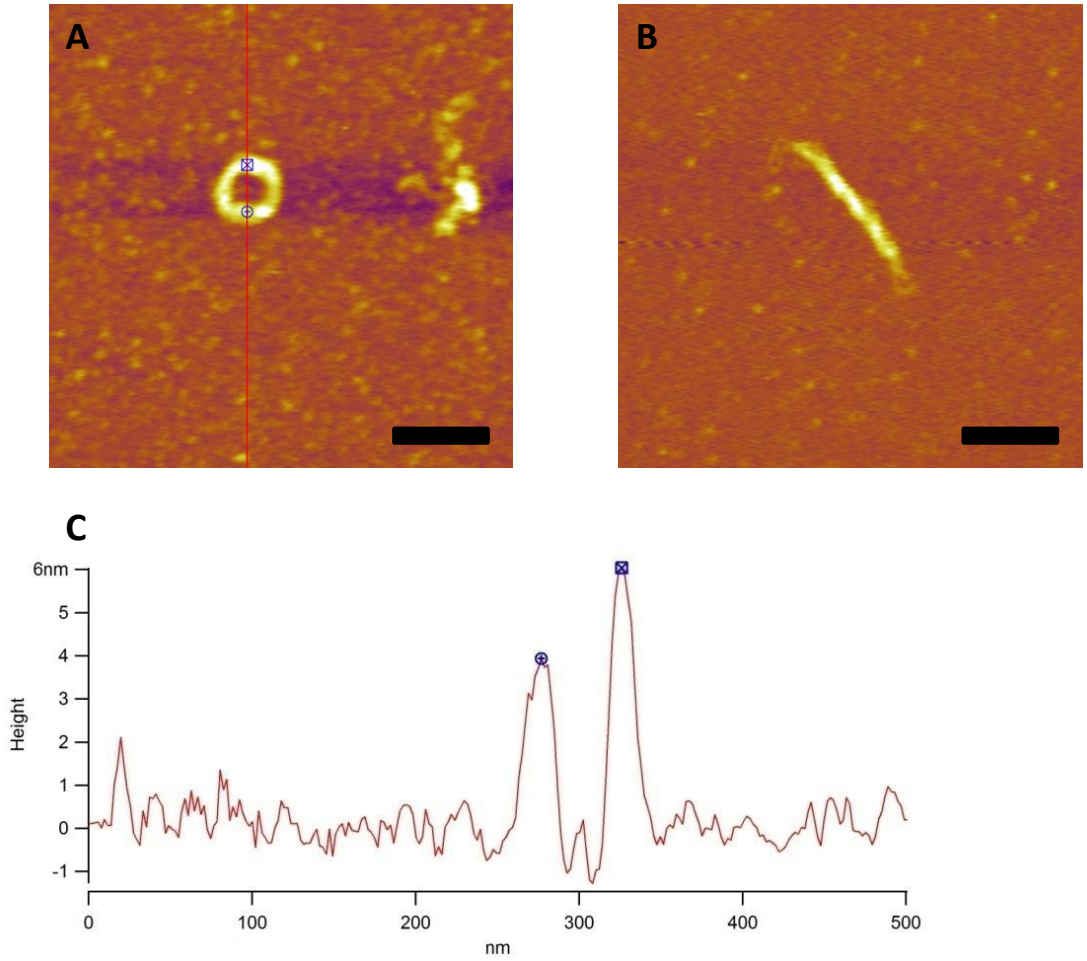

Figure 3.4 PEI condenses DNA into rods and toroids
AFM images showing a magnified view of a toroidal complex (**A**) and a rod-shaped condensed plasmid (**B**) on PEI-coated mica. The height trace (**C**) corresponds to the line drawn in (**A**), showing the height peaks which were used to measure the diameter of the toroid. Scale bar
represents 100 nm.

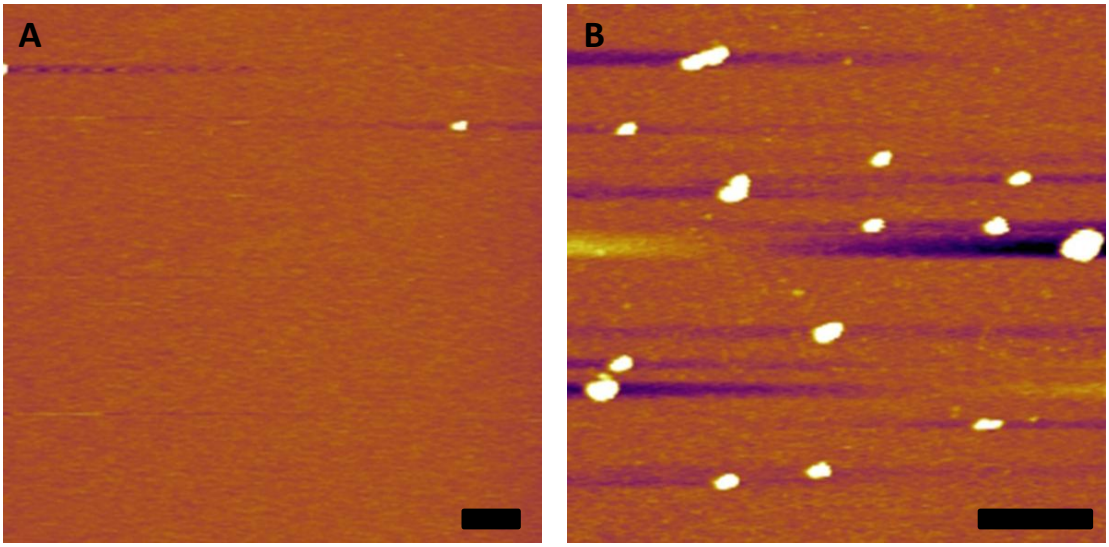

Figure 3.5 PEI polyplexes are globular at higher N/P ratios
PEI-DNA complexes prepared at N/P ~2 (A) and 20 (B) then deposited on bare mica. All complexes observed were globular in appearance, and average width of ~ 80 nm. Scale bar is 500 nm.

3.3.2 PEI-DNA complexes characterized by DLS and zeta potential

Control measurements were done on naked plasmids at the same concentration (20 mg/L) used to prepare the complexes, as well as the PEI on its own (data not shown). Due to the low concentration and insufficient scattering of the individual species, no reliable DLS data was obtained. Thus, it is very likely that the measurements done on the complexes correspond only to the condensed species such as those seen in AFM. Size measurements from DLS give a hydrodynamic radius of 104 ± 25 nm at N/P ~ 1 (Figure 3.6). This corresponds reasonably well with the AFM data considering the sizes of the rods and toroids that were observed. At N/P ~ 3, the particle diameter increases to 860 ± 151 nm, indicating aggregation of the complexes. Interestingly, the zeta potential crosses from negative to positive as the N/P ratio increases from 2 to 4. The size increase is therefore likely due to

aggregation arising from insufficient electrostatic repulsion between the condensates. As the N/P ratio is further increased, the zeta potential rises to 18.3 ± 1.2 mV and the particle diameter decreases to 167 ± 18 nm. Further addition of PEI shows no significant affect on the complexes (data not shown). As evidenced by AFM, these sizes correspond to the positively charged globular morphologies seen to adsorb on the bare mica.

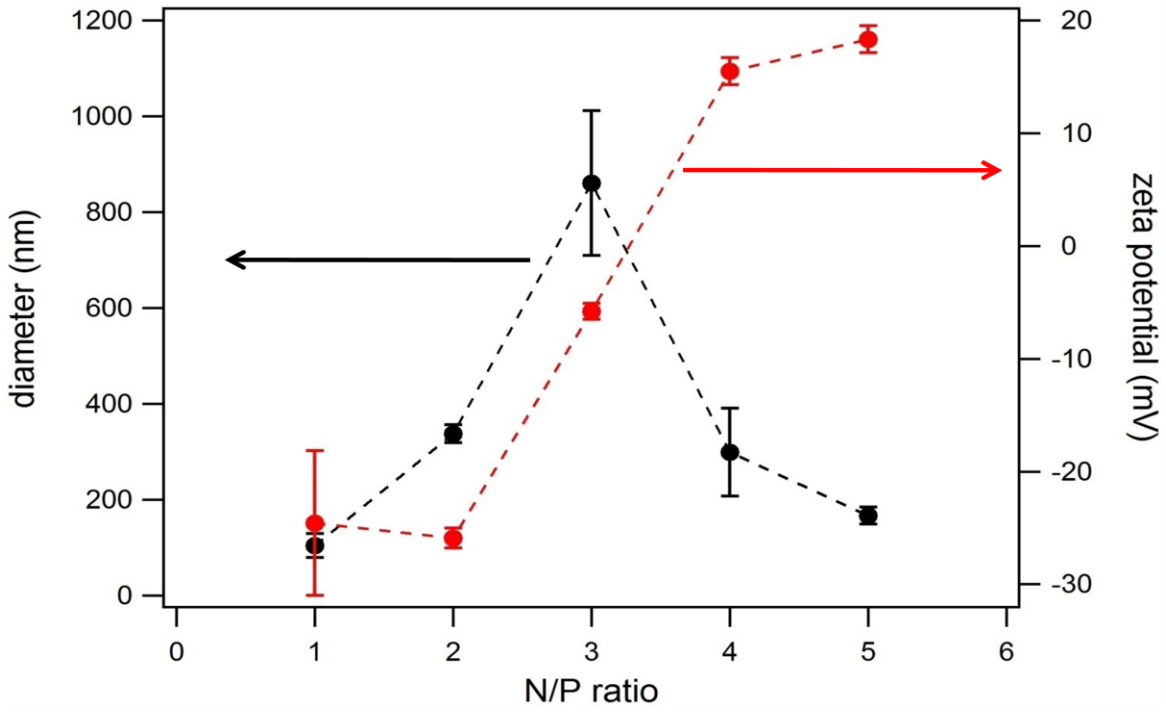

Figure 3.6 DLS and zeta potential data for PEI polyplexes
Size (**black**) and zeta potentials (**red**) for PEI-DNA complexes prepared as in section 3.2.3. The spike in size corresponds with the zeta potential approaching 0. As the complexes gain a higher positive surface charge, the polyplexes are able to stabilize into < 200 nm particles.

3.4 Discussion

As expected based on previous studies, PEI has shown excellent capability in binding with DNA and forming compact structures. The morphologies of these

condensates however, strongly depend on the relative concentrations of PEI to the plasmid. At the lower N/P ratios, initial condensates assume rod-like or toroidal morphologies as well as some small globular complexes. The rods and toroids formed with PEI are very similar to those reported in the literature from DNA condensed with not only PEI, but a variety of other condensing agents such as PLL, cobalt hexamine, and other organic cations [6], [8], [57], [58]. The rods and toroids were only observed at N/P < 2, on PEI-coated mica. Because of the slight negative overall charge of rods and toroids [59], coating the normally negatively charged mica surface with PEI was necessary to image them in aqueous conditions. Using divalent ions such as Mg^{2+} or Ni^{2+} , which are often used to promote adsorption of DNA to mica, failed to show any rods/toroids at all N/P ratios tested. With pre-adsorbed PEI on the mica surface, however, the polyplexes readily bound to the surface while having little affect on the condensation process as evidenced by Figure 3.3a.

As N/P ratio is further increased, we see a transition from negative to positively charged polyplexes at N/P ~ 3. Near this transition region (close to neutral charge), the complexes aggregate and are much larger due to lack of electrostatic repulsion between the particles. In the positive charge regime, we no longer observe rods and toroids, but only globular complexes in AFM. These complexes only adsorb on the negatively charged bare mica, while nothing is observed on the PEI-coated mica. The size of these globular polyplexes measured via DLS (167 ± 18 nm) agrees reasonably well with what others have reported for PEI-DNA complexes [60]. While the average size measured through AFM observations is significantly smaller (~80 nm in width), the discrepancy may be mostly explained due to the heterogeneity in

size, which leads to the intensity-based average from DLS to be larger than the number-based average when measuring from AFM data.

The overall trend here of smaller to large to small complexes roughly mirrors the results of one study using 13 kDa linear PEI [55]. In this study, they reported the formation of ~20 nm complexes alongside partially or uncondensed DNA at the lower N/P ratios in their AFM observations. At N/P ~ 2, they noticed that the complexes appeared to merge and grow in size, and stable ~200 nm particles formed at N/P > 10. While no rods or toroids were observed at any N/P values, this may be due to the differences in condensing agents, as well as the AFM methods which were done in air. Zeta potential measurements of 25 kDa branched PEI polyplexes were also reported by Bettinger et al. [56]. The neutrality point occurred at N/P ~ 4 while here we measured the charge reversal to occur at approximately N/P ratio of 3. The zeta potential at the higher N/P ratios leveled off just below +20 mV which agrees well with our data.

It is unclear, however, how the formation of rods and toroids relates to the globular complexes we see at higher N/P values. Rods and toroids often consist of multiple DNA molecules, and can continue to grow thicker as more DNA is accumulated. Sometimes toroids can grow thick enough where the central hole is barely visible. It is reasonable to assume that at some point, they lose their toroidal appearance as more DNA is added onto the particle, but there is little evidence for this in the data presented here. Also, some small, globular morphologies can already be seen in the negative zeta potential regime (Figure 3.3), which suggests they may be an entirely different primary morphology. Whether a toroid or globular particle is

formed may simply depend on the number of PEI molecules per DNA. An excess of PEI molecules may disrupt the formation of neatly stacked rods or toroids due to geometric constraints and/or multiple random DNA sites bridged by PEI molecules. To better understand the evolution of these polyplexes, a study focused more on the kinetics of complex formation could provide more insight, as well as potentially better control over the formation of the desired morphologies.

Chapter 4: DNA condensation with HK peptide

4.1 Introduction

Several publications have shown that histidine-lysine (HK) peptides can be effective nucleic acid carriers [34]–[36]. The lysine residues interact with the negatively charged phosphate groups of the DNA while the histidine component provides a pH buffering capability to assist with endosomal escape. One variation of the HK polymer is H2K4b; a four-branched polymer with a repeating pattern of -HHK-. The H2K4b polymer was shown to have higher transfection efficiencies *in vitro* compared to linear and -HK- variants [61]. Linear HK polymers, on the other hand, were only capable of enhancing transfection *in vitro* when combined with liposomes [62]. An eight-branched variation (H3K8b) has also been studied and shown to be more effective as an siRNA carrier, but less effective as a plasmid carrier than the four-branched HK polymers [34]. H3K variants have a higher histidine:lysine ratio which should result in a greater chance for endosomal lysis. The higher histidine:lysine ratio, however, also means the HK polymer will have a lower charge density at physiological pH which may affect the stability of the polyplex. That being said, one must keep in mind the delicate balance between polyplex stability and its ability to release its genetic cargo for successful transfection to occur.

The relationship between the physical characteristics such as polyplex size and surface charge, and transfection efficiency is yet to be fully understood. While some physical characterization was done on some of the HK complexes [44], the authors were unable to draw any real connections to their transfection behavior.

Here, we will be looking specifically at a four-branched HK variant, H3K(+G)4b and its complexation with DNA. We will carefully examine the physical characteristics using AFM as well as DLS and zeta potential measurements, and attempt to follow its condensation process.

4.2 Materials and Methods

The histidine-lysine peptide used here has four branches around a three-lysine core with each branch having a repeating sequence of HHHK (Figure 4.1). From here onward, this peptide is referred to as H3K(+G)4b or simply HK. Its molecular weight is ~ 10 kDa and contains about 80 residues. It was synthesized with a Rainin Voyager synthesizer (PTI, Tucson, AZ) by Mixson's group [62]. The polymers were purified on an HPLC (Beckman, Fullerton, CA) and analyzed with mass spectroscopy (PerSeptive Biosystems, Foster City, CA) to verify the predicted molecular weight. Glycine was inserted after every 9^{th} amino acid in order to increase the yield. The procedures here are similar as those described in section 3.2 with the exception that we are now using the HK polymer instead of PEI. The plasmid DNA (pBR322, New England BioLabs) is diluted to 20 μg/mL in a 10 mM Tris buffer (pH 7.4) solution. The plasmid solution is then added to a solution of equal volume with appropriately diluted HK in 10 mM Tris buffer to obtain the desired N/P ratio. The mixture is gently vortexed for 10 seconds then incubated at room temperature for 30 min. After incubation, 80 μL of the complex solution is dropped onto a freshly cleaved mica surface or a HK-coated mica surface. For the low pH experiments, the Tris buffer is replaced with 10 mM citrate buffer (pH 5).

To coat the mica surface with HK, a 10 μL droplet of 10 μM HK is deposited on freshly cleaved mica and incubated for 5 min. The coated mica is then rinsed by adding 100 μL of the buffer solution, incubated for 1 min, then removed by the pipette. This is repeated five more times to ensure there is a negligible amount of the excess, unbound HK present in the solution. Samples prepared for AFM imaging were deposited on both HK-coated mica as well as bare mica in order to observe both positively and negatively charged species on the surface.

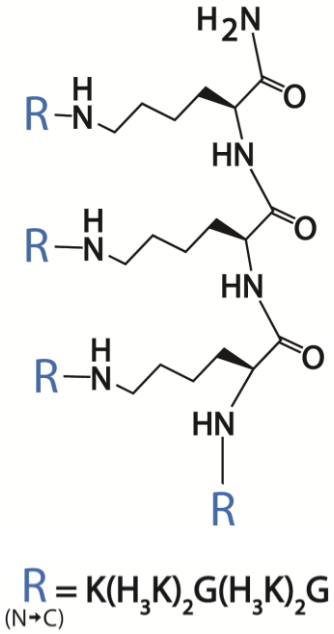

Figure 4.1 Structure of the HK peptide, showing a three lysine core and the amino acid sequence for each branch

4.3 Results

4.3.1 HK-DNA complex formation at physiological pH

AFM images of HK-DNA complexes at various N/P ratios in Tris buffer (pH 7.4) are shown in Figure 4.2. A significant amount of condensed DNA appears to form at an N/P ratio of 2, although the majority still appears to be uncondensed. The condensed DNA assumes toroidal or rod-like morphologies just as with PEI. As the N/P ratio is increased to 3 and 4, the amount of uncondensed DNA relative to the condensed structures observed in the AFM images gradually decreases. Furthermore, the appearance of taller, and thicker (greater z-height and lateral width) toroids and rods become more common (Figure 4.2c). As the N/P ratio is further increased, the complexes begin to cluster together in certain areas and larger aggregates are observed. The diameter of the toroids were measured to be 56 ± 9 nm and the length of the rods were 176 ± 52 nm. It should be noted that all of these images were obtained when using HK-coated mica, whereas no particles or DNA were seen from solution deposited on bare mica.

Size and zeta potential measurements were also performed on the HK complexes over the same N/P range as shown in Figure 4.3. At N/P = 2 the measured hydrodynamic diameter was 117 ± 14 nm. This size corresponds fairly well with the sizes of the rods and toroids that were observed via AFM. The signal is presumed to be due to the condensed structures since uncondensed DNA at the concentrations being used here is not observable by DLS due to the very low scattering signal. As the N/P ratio increases to 3 and 4, the size increases dramatically to 670 ± 43 nm and 951 ± 82 nm, respectively. While large aggregates were rarely observed by AFM at

these N/P ratios, large aggregates scatter much more strongly than the smaller particles so the larger sizes dominate the DLS measurement even though smaller condensates may be more prevalent in number as suggested by AFM. As the N/P ratio is further increased, the size plateaus at around a micron which suggests the complexes simply aggregate and probably precipitate as more HK is added.

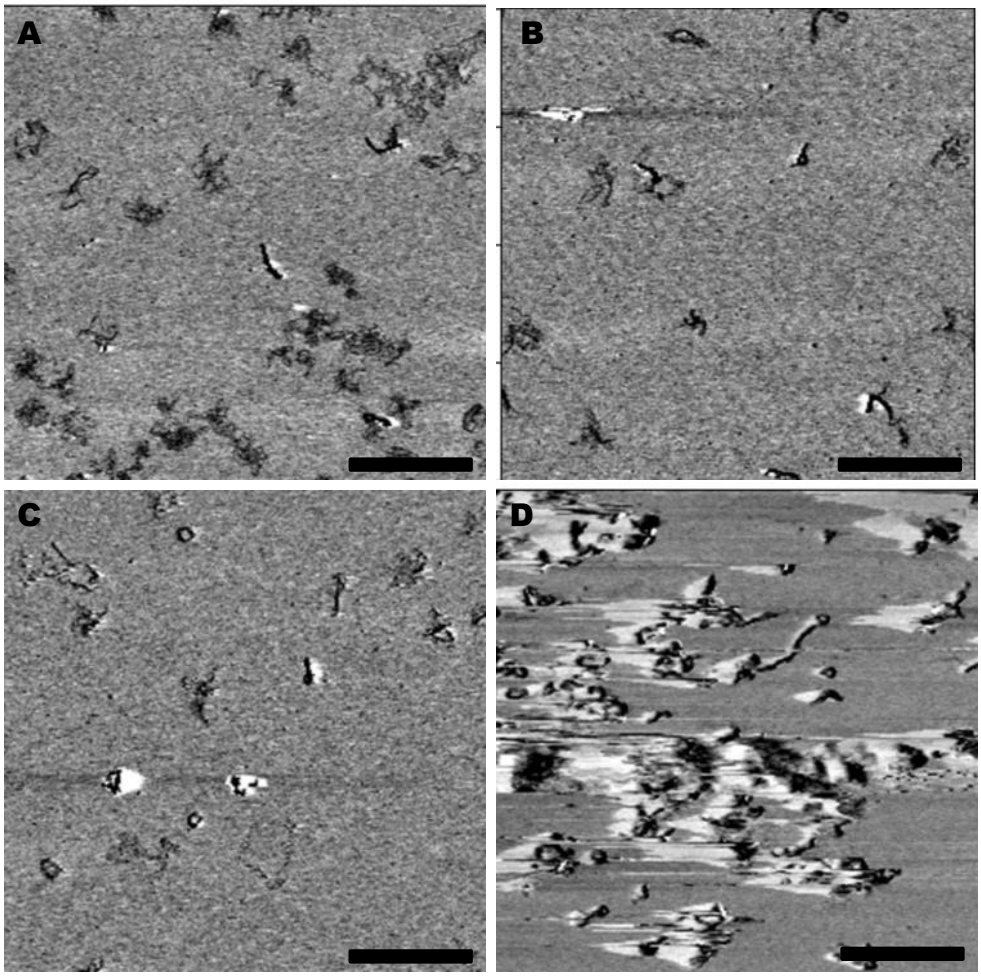

Figure 4.2 AFM images of DNA complexes condensed with HK
HK-DNA complexes were prepared at N/P ~ 2 (**A**), 3 (**B**), 4 (**C**), 5 (**D**), and incubated for 30 min prior to depositing on HK-coated mica. As N/P ratio increases, an increasing fraction of the DNA is condensed into rods, toroids and globular structures. At N/P > 4, large aggregates and clusters of complexes became common as seen in (**D**). Scale bar is 500 nm.

The zeta potential data (Figure 4.3) shows that the complexes have an overall negative charge until N/P ~ 6. This corresponds well with the fact that no complexes were observed via AFM on the negatively charged bare mica surface. As expected, the zeta potential increases as more HK is added and therefore adding more positive charge to the complexes. While the complexes are somewhat charged, the zeta potential values for N/P > 3 are close to neutral or only slightly positive that the fact that the complexes are aggregating is not surprising.

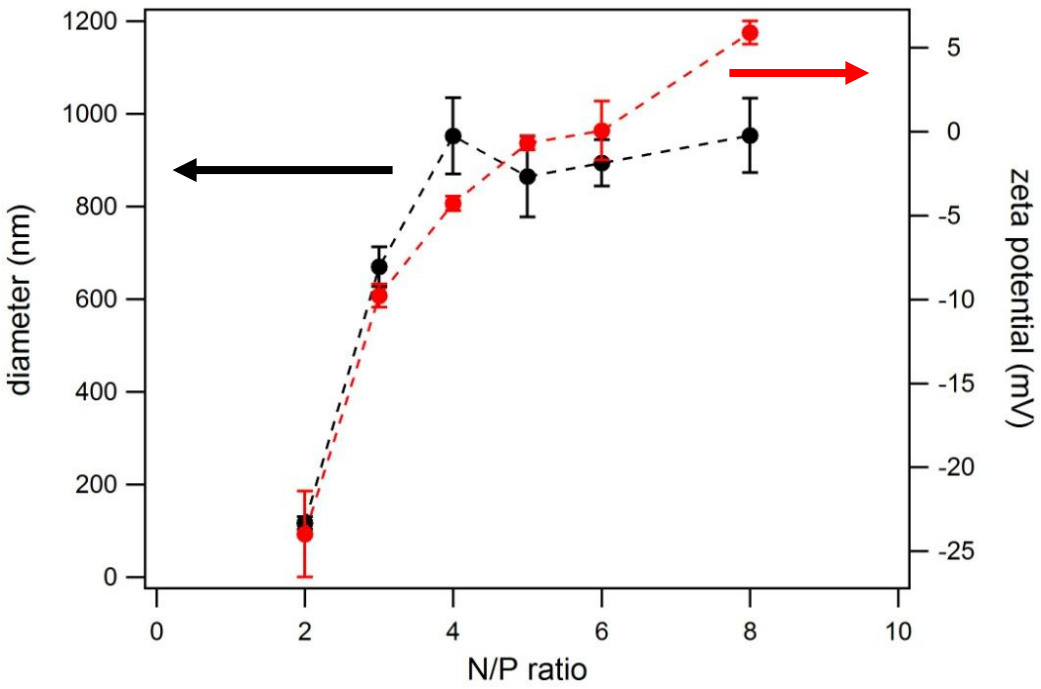

Figure 4.3 DLS and zeta potentials for HK-DNA complexes at pH 7.4
The size of the complexes (black curve) increases rapidly from 117 nm to nearly a micron as the zeta potential (red curve) shows a corresponding neutralization of the complexes.

4.3.2 HK-DNA complexes formed at pH 5

The H3K(+G)4b polymer is designed to have a strong pH buffering effect which may be useful for endosomal escape and transfection. To see the effects of pH and the histidine charges on polyplex formation, DNA-HK complexes were prepared in citrate buffer (pH 5.0). Unlike polyplexes prepared at pH 7.4, a significant portion of the DNA molecules appear to be condensing at an N/P ratio of only 0.5. The condensed morphologies consist of rods, toroids, and globular structures (Figure 4.4). As expected, the fraction of condensed DNA molecules steadily increases with N/P ratio. At N/P ~ 2 we begin to notice a depletion of uncondensed DNA and complexes, and start to observe only a few globular structures on the HK-coated mica surface. At higher N/P ratios, complexes are only observed when deposited on the negatively charged, bare mica. Here, we see what appears to be simply large aggregates that are a few microns across but closer inspection shows an internal granular structure (Figure 4.4d). The particles that can be isolated appear to be roughly 200 nm in height as well as width with some distribution.

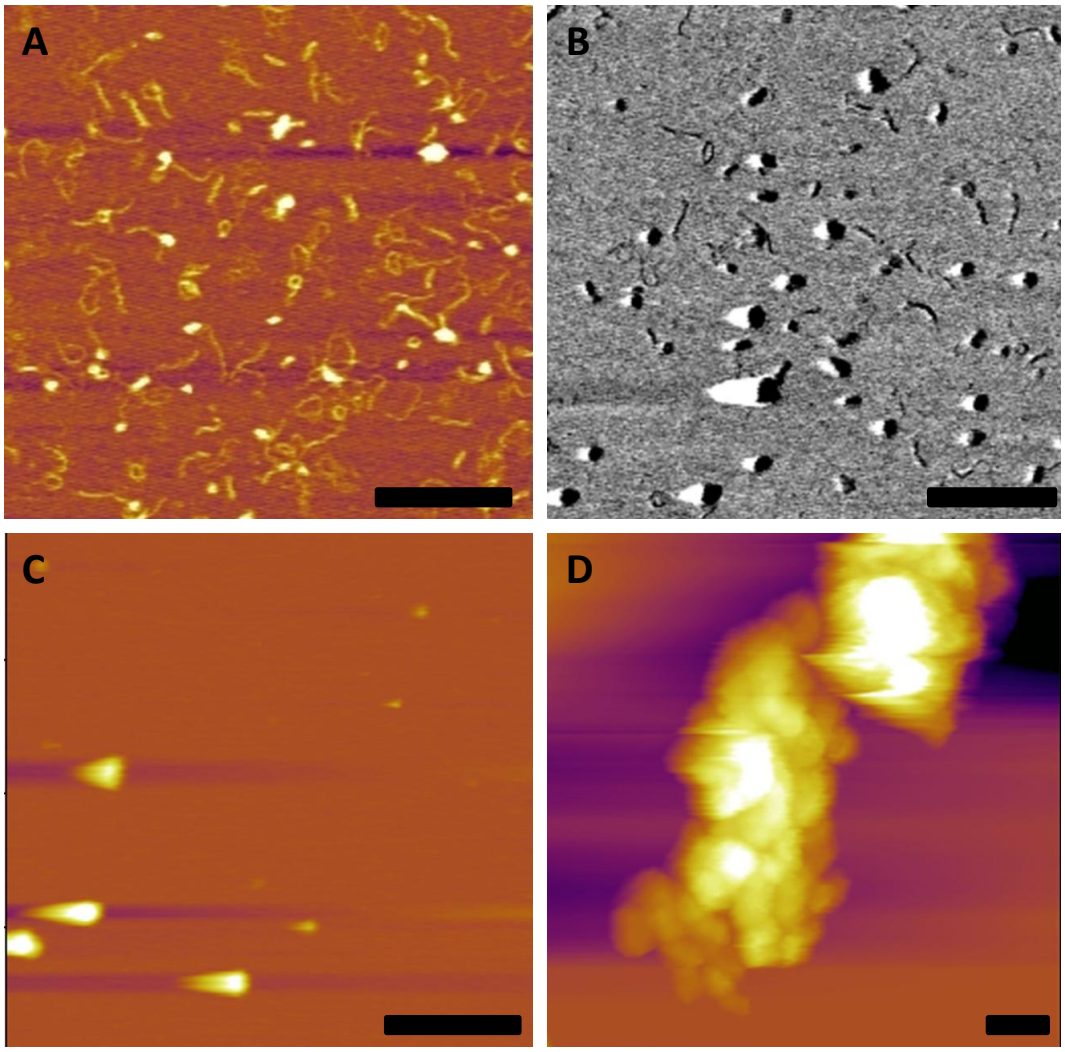

Figure 4.4 AFM images of HK-DNA complexes at pH 5
HK and DNA were mixed and incubated at N/P ~ 0.5 (**A**), 1.0 (**B**), 2.0 (**C**), and 6.0 (**D**) prior to depositing on HK-coated mica (**A-C**) or bare mica (**D**). Formation of rods and toroids can be seen in (**A**) and (**B**) while only globular morphologies appear at N/P ~ 2 (**C**). At higher N/P ratios the complexes only adhere to the negatively charged, bare mica and would mostly cluster together (**D**). Scale bar is 500 nm.

DLS measurements show particle sizes of about 150 - 200 nm while the N/P ratio is between 1.5 and 2.25 (Figure 4.5). Below 1.5, the scattering intensity was not large enough to produce reliable data. At N/P ~ 2.25, there is a spike in the size of the complexes followed by a drop-off that plateaus at approximately 300 nm for N/P > 4. Likewise, the zeta potential of the complexes rapidly increases between N/P

ratios of 2.0 and 2.5, going from negative to positive. This corresponds very well with the spike seen in the size measurements, and shows there is a fairly small transition region where the complexes aggregate due to their neutralization. As the N/P ratio is further increased, the zeta potential seems to increase until it levels off at ~ 12 mV for N/P > 5. The change in sign of the surface charge also corresponds with the fact that complexes can only be seen when deposited on bare mica at the higher N/P ratios. Also, it is interesting to note that the size of the granules that make up the large clusters seen in the AFM images are roughly similar to the particle diameters measured by DLS for the same N/P ratios.

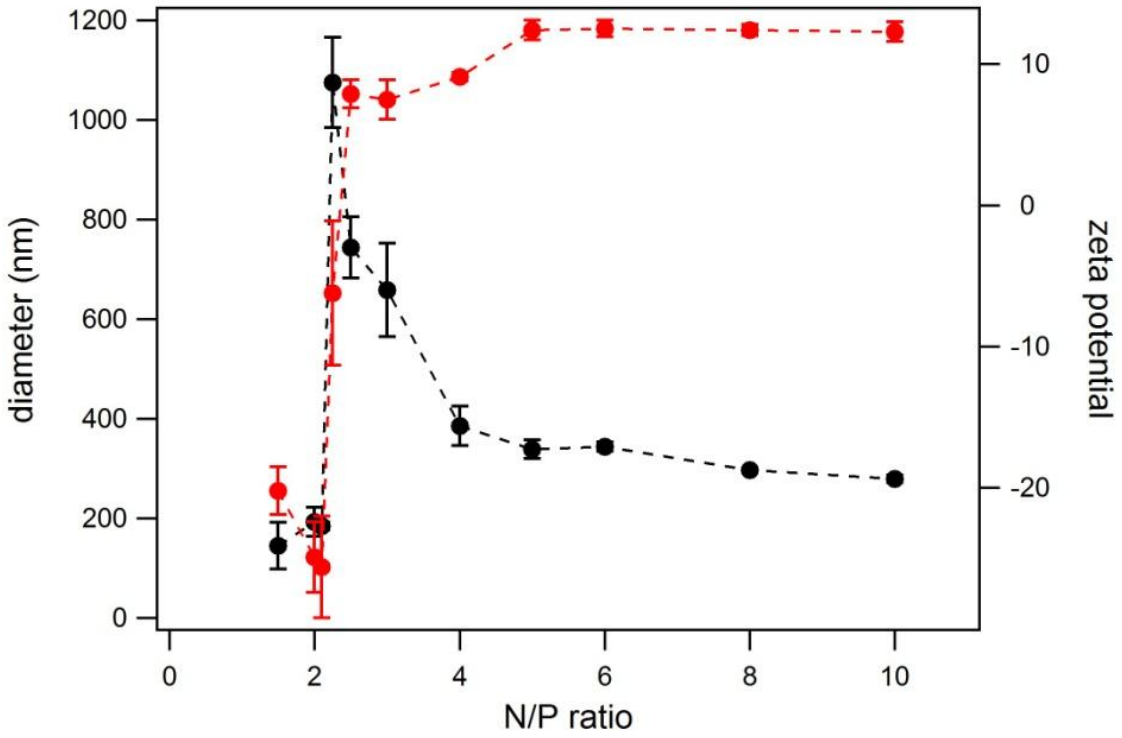

Figure 4.5 DLS and zeta potentials for HK-DNA complexes at pH 5
Complexes prepared in citrate buffer show a sudden spike in diameter (black curve) between N/P 2 and 2.5, which corresponds with a spike in zeta potential (red curve) and charge reversal. As the zeta potential plateaus at ~ 12 mV, the particle diameter decreases and levels off at ~ 300 nm.

4.4 Discussion

The morphologies of the complexes in the initial stages of condensation at both pH 7.4 and pH 5 are similar, in that they both consist of rods, toroids, and some globular structures. No significant differences in rod and toroid sizes were seen between the two conditions, as well as with those formed with PEI as shown in chapter 3. Furthermore, the sizes of the observed rods and toroids are consistent with those reported by others in the literature using a variety of other condensing agents [6], [12], [56], [57]. In general, rod and toroidal structures will tend to form when DNA is complexed with small, polycationic agents with sufficient charge density, given the right conditions. The fact that the sizes of these morphologies do not differ much between the various cationic agents and conditions should not be too surprising, as the formation of rod and toroidal structures is more of an intrinsic property of the DNA molecule itself.

The aggregation of the complexes with HK at pH 7.4 can be attributed to their low surface charge as evidenced by the zeta potential data. In general, particles that rely on electrostatic repulsion to remain stable in solution for long periods of time require zeta potentials of > 30 mV or < -30 mV [63]. While the complexes formed at pH 5.0 also do no reach this zeta potential, they are significantly more charged at the higher N/P ratios compared to the complexes formed at pH 7.4. This surface charge seems to be enough to prevent initial aggregation, and form distinct, nano-sized particles. It should be noted however, that while attempting to image these particles with AFM, they consistently appeared in clusters on the mica surface. Due to the DLS data, and the fact that these clusters were microns in width while only a few

hundred nanometers in height, it seems unlikely that clusters of such size were forming in solution prior to depositing on the mica. One possible explanation is that the interaction of the complexes with the mica surface leads to partial neutralization which helps promote the localization of more particles around the area. However, even in solution the complexes were not stable for longer periods of time. When attempting to gather data from AFM or DLS after incubating the samples (N/P > 3, pH 5) for 24 hr, nothing was observed, likely due to further aggregation and precipitation of the complexes to the bottom of the centrifuge tube.

Overall the data clearly shows a significant effect on the complex formation process due to pH. At physiological pH, the majority of the histidines (pKa ~ 6) remain uncharged. With each HK molecule consisting of 23 lysines, and 48 histidines, this is a significant portion of the potential total charge. It is therefore reasonable to see the condensation process occur at much lower N/P ratios when the complexes were prepared at pH 5, due to a lower number of HK molecules required to neutralize the DNA charge as the histidine residues are charged. The larger amount of HK molecules required to condense DNA at pH 7.4 may also be the reason the complexes are unable to stabilize into nanoparticles regardless of how much HK continues to be added. Due to density limitations, there is a point of HK saturation in the complex and any further addition of HK remains unbound in solution. This is evident by the plateau behavior in the DLS and zeta potential data. At pH 7.4, the DNA becomes saturated with HK at a point where the charge on the complex is roughly neutral, and therefore aggregates. At pH 5, due to the additional histidine

charges, the DNA complex gains an overall positive charge at its HK saturation point which leads to nanoparticles, but these appear to be only stable for several hours.

Due to significant aggregation of the HK complexes at physiological pH at the higher N/P ratios, they would likely be ineffective for transfection purposes. The nano-sized rods and toroids formed at the lower N/P ratios, however, may possibly be useful for transfection. Although negatively charged, some publications have shown that rod-shaped morphologies can be effective at entering cells. Leng et. al. has shown via TEM imaging, the presence of "needle-like" HK complexes inside the cells [44]. We have also demonstrated a significant pH effect due to the histidine which could prove useful in the endosomal lysing process.

Chapter 5: Further discussion and future directions

5.1 Transfection efficiencies

Ultimately, we would like to correlate the physical characterization data with cell transfection behavior. While PEI polyplexes have been studied often in the literature, the morphological variations across N/P ratios have not been fully appreciated yet. Here, it has been shown that rod and toroidal complexes are only observed at N/P < 2 where they still carry an overall negative surface charge. Then there is a transition region at N/P ~ 3 where the polyplexes aggregate, followed by formation of ~ 170 nm globular structures which are positively charged at higher N/P ratios. It would be insightful to test the transfection efficiencies of the PEI polyplexes at the lower N/P ratios even though there would still be some free DNA in the solution, and how it compares to the fully complexed DNA at the higher N/P ratios. The rod-like morphologies may be useful for transfection as observed by Leng et al. [44]. Furthermore there may be substantial differences in toxicity levels across the N/P ratios as unmodified PEI is typically cited as a highly cytotoxic transfection agent.

Likewise, it would be interesting to test the transfection capabilities of the H3K(+G)4b polymer across the N/P ratios characterized herein. Currently no work regarding the transfection of this particular HK peptide has been published. While some transfection results have been published regarding other HK variants [34], [35], [38], [61], it is not yet clear what properties of the complexes are ideal. For example, the four-branched HK polymer was initially shown to be superior to linear HK [35],

but later experiments had the linear HK outperforming the branched variation, and negatively charged complexes were surprisingly effective [64]. While differing conditions may explain the differences, it may also be due to a lack of appreciation for the various species that may exist within a polyplex solution, and which actually contribute to its observed transfection behavior.

5.2 Complex preparation on flat substrates

Preparing DNA carriers on a flat substrate may not only be useful for imaging purposes but for transfection as well. Chang et al. has shown cellular uptake of genetic material by adding a cell-DNA mixture onto a PEI/collagen-coated substrate which they termed "surfection" [65]. This shows there is potential for first preparing the complexes on a substrate which can be imaged directly by AFM, and also carry out *in vitro* transfection experiments by depositing the cells on the complex-coated substrate. This may have the advantage of being able to more precisely tune the amount of complex material per cell in order to optimize uptake of genetic material while minimizing toxicity. Furthermore, one may be interested in the transfection properties of certain complex morphologies that optimally form on a surface rather than in solution.

By first dispersing the DNA molecules or condensing agent across a surface, it may also be possible to form single DNA molecule complexes or a more homogeneous distribution of complex sizes and morphologies. Such a method may improve the transfection behavior of a gene delivery vehicle by limiting the amount

of DNA complex structures with unwanted properties. At the very least, improved homogeneity of the complex distribution will help in better understanding the correlation between the physical properties of a complex and its ability to transfect. A heterogenous distribution such as that observed with the AuNP-DNA complexes in 4.3.1, may result in misled conclusions if one looks at the average physical properties, but the transfection behavior is actually dominated by a small subset of the overall population. If a surface-based complex formation process is used, however, it will be necessary to also develop methods to detach the complexes from the substrate while keeping the complexes intact in order to be useful for *in vivo* applications.

Bibliography

[1] P. Carrivain, A. Cournac, C. Lavelle, A. Lesne, J. Mozziconacci, F. Paillusson, L. Signon, J.-M. Victor, and M. Barbi, "Electrostatics of DNA compaction in viruses, bacteria and eukaryotes: functional insights and evolutionary perspective," *Soft Matter*, vol. 8, no. 36, p. 9285, 2012.

[2] S. Mantelli, P. Muller, S. Harlepp, and M. Maaloum, "Conformational analysis and estimation of the persistence length of DNA using atomic force microscopy in solution," *Soft Matter*, vol. 7, no. 7, p. 3412, 2011.

[3] A. Savelyev, C. K. Materese, and G. A. Papoian, "Is DNA's rigidity dominated by electrostatic or nonelectrostatic interactions?," *J. Am. Chem. Soc.*, vol. 133, no. 48, pp. 19290–19293, 2011.

[4] V. A. Bloomfield, "DNA condensation," *Curr. Opin. Struct. Biol.*, vol. 6, pp. 334–341, 1996.

[5] a a Kornyshev and S. Leikin, "Electrostatic Zipper Motif for DNA Aggregation," *Phys. Rev. Lett.*, vol. 82, no. 20, pp. 4138–4141, 1999.

[6] G. Liu, M. Molas, G. A. Grossmann, M. Pasumarthy, J. C. Perales, M. J. Cooper, and R. W. Hanson, "Biological Properties of Poly-L-lysine-DNA Complexes Generated by Cooperative Binding of the Polycation," *J. Biol. Chem.*, vol. 276, no. 37, pp. 34379–34387, 2001.

[7] D. K. Chattoraj, L. C. Gowle~, and J. A. Schellman, "DNA Condensation with Polyamines II. Electron Microscopic Studies," *J. Mol. Biol*, vol. 121, pp. 327–337, 1978.

[8] C. C. Conwell and N. V Hud, "Evidence That Both Kinetic and Thermodynamic Factors Govern DNA Toroid Dimensions: Effects of Magnesium(II) on DNA Condensation by Hexammine Cobalt(III)," *Biochemistry*, vol. 43, no. 18, pp. 5380–5387, 2004.

[9] M. E. Cerritelli, N. Cheng, A. H. Rosenberg, C. E. Mcpherson, F. P. Booy, and A. C. Steven, "Encapsidated Conformation of Bacteriophage T7 DNA," *Cell*, vol. 91, pp. 271–280, 1997.

[10] N. V Hud, K. H. Downingt, and R. Balhorn, "A constant radius of curvature model for the organization of DNA in toroidal condensates," *Biophysics (Oxf).*, vol. 92, pp. 3581–3585, 1995.

[11] R. Cortini, B. R. Caré, J. M. Victor, and M. Barbi, "Theory and simulations of toroidal and rod-like structures in single-molecule DNA condensation," *J. Chem. Phys.*, vol. 142, no. 10, 2015.

[12] I. D. Vilfan, C. C. Conwell, T. Sarkar, and N. V Hud, "Time study of DNA condensate morphology: Implications regarding the nucleation, growth, and equilibrium populations of toroids and rods," *Biochemistry*, vol. 45, no. 26, pp. 8174–8183, 2006.

[13] A. A. Zinchenko, T. Sakaue, S. Araki, K. Yoshikawa, and D. Baigl, "Single-chain compaction of long duplex DNA by cationic nanoparticles: Modes of

interaction and comparison with chromatin," *J. Phys. Chem. B*, vol. 111, no. 11, pp. 3019–3031, 2007.

[14] L. B. Jensen, K. Mortensen, G. M. Pavan, M. R. Kasimova, D. K. Jensen, V. Gadzhyeva, H. M. Nielsen, and C. Foged, "Molecular characterization of the interaction between siRNA and PAMAM G7 dendrimers by SAXS, ITC, and molecular dynamics simulations," *Biomacromolecules*, vol. 11, no. 12, pp. 3571–3577, 2010.

[15] R. K. DeLong, C. M. Reynolds, Y. Malcolm, A. Schaeffer, T. Severs, and A. Wanekaya, "Functionalized gold nanoparticles for the binding, stabilization, and delivery of therapeutic DNA, RNA, and other biological macromolecules," *Nanotechnol. Sci. Appl.*, vol. 3, no. 1, pp. 53–63, 2010.

[16] N. V Hud and I. D. Vilfan, "Toroidal DNA condensates: unraveling the fine structure and the role of nucleation in determining size.," *Annu. Rev. Biophys. Biomol. Struct.*, vol. 34, pp. 295–318, 2005.

[17] D. W. Pack, A. S. Hoffman, S. Pun, and P. S. Stayton, "Design and development of polymers for gene delivery.," *Nat. Rev. Drug Discov.*, vol. 4, no. 7, pp. 581–93, 2005.

[18] H. Yin, R. L. Kanasty, A. a Eltoukhy, A. J. Vegas, J. R. Dorkin, and D. G. Anderson, "Non-viral vectors for gene-based therapy.," *Nat. Rev. Genet.*, vol. 15, no. 8, pp. 541–555, 2014.

[19] N. Bessis, F. J. GarciaCozar, and M.-C. Boissier, "Immune responses to gene therapy vectors: influence on vector function and effector mechanisms.," *Gene Ther.*, vol. 11 Suppl 1, pp. S10-7, Oct. 2004.

[20] D. Bouard, D. Alazard-Dany, and F.-L. Cosset, "Viral vectors: from virology to transgene expression.," *Br. J. Pharmacol.*, vol. 157, no. 2, pp. 153–65, May 2009.

[21] M. Morille, C. Passirani, A. Vonarbourg, A. Clavreul, and J. P. Benoit, "Progress in developing cationic vectors for non-viral systemic gene therapy against cancer," *Biomaterials*, vol. 29, no. 24–25. pp. 3477–3496, 2008.

[22] S. Mukherjee, R. N. Ghosh, and F. R. Maxfield, "Endocytosis.," *Physiol. Rev.*, vol. 77, no. 3, pp. 759–803, Jul. 1997.

[23] L. Wasungu and D. Hoekstra, "Cationic lipids, lipoplexes and intracellular delivery of genes.," *J. Control. Release*, vol. 116, no. 2, pp. 255–64, Nov. 2006.

[24] J. Behr, "The proton sponge: a trick to enter cells the viruses did not exploit," *Int. J. Chem.*, vol. 2, no. 1, pp. 34–36, 1997.

[25] C. L. Grigsby and K. W. Leong, "Balancing protection and release of DNA: tools to address a bottleneck of non-viral gene delivery," *J. R. Soc. Interface*, vol. 7, no. Suppl 1, pp. S67–S82, 2010.

[26] H. Pollard, G. Toumaniantz, J. L. Amos, H. Avet-Loiseau, G. Guihard, J. P. Behr, and D. Escande, "Ca2+-sensitive cytosolic nucleases prevent efficient delivery to the nucleus of injected plasmids," *J. Gene Med.*, vol. 3, no. 2, pp. 153–164, 2001.

[27] D. V Schaffer, N. A. Fidelman, N. Dan, and D. A. Lauffenburger, "Vector unpacking as a potential barrier for receptor-mediated polyplex gene delivery," *Biotechnol. Bioeng.*, vol. 67, no. 5, pp. 598–606, Mar. 2000.

[28] C. Plank, B. Oberhauser, K. Mechtler, C. Koch, and E. Wagner, "The influence of endosome-disruptive peptides on gene transfer using synthetic virus-like gene transfer systems," *J. Biol. Chem.*, vol. 269, no. 17, pp. 12918–12924, Apr. 1994.

[29] W. . Godbey and A. . Mikos, "Recent progress in gene delivery using non-viral transfer complexes," *J. Control. Release*, vol. 72, no. 1, pp. 115–125, 2001.

[30] H. Lv, S. Zhang, B. Wang, S. Cui, and J. Yan, "Toxicity of cationic lipids and cationic polymers in gene delivery.," *J. Control. Release*, vol. 114, no. 1, pp. 100–9, Aug. 2006.

[31] M. Glodde, S. R. Sirsi, and G. J. Lutz, "Physiochemical properties of low and high molecular weight poly(ethylene glycol)-grafted poly(ethylene imine) copolymers and their complexes with oligonucleotides," *Biomacromolecules*, vol. 7, no. 1, pp. 347–356, 2006.

[32] L. Wightman, R. Kircheis, V. Rössler, S. Garotta, R. Ruzicka, M. Kursa, and E. Wagner, "Different behavior of branched and linear polyethylenimine for gene delivery in vitro and in vivo," *J. Gene Med.*, vol. 3, no. 4, pp. 362–372, 2001.

[33] H. Petersen, P. M. Fechner, A. L. Martin, K. Kunath, S. Stolnik, C. J. Roberts, D. Fischer, M. C. Davies, and T. Kissel, "Polyethylenimine-graft-poly(ethylene glycol) copolymers: Influence of copolymer block structure on DNA complexation and biological activities as gene delivery system," *Bioconjug. Chem.*, vol. 13, no. 4, pp. 845–854, 2002.

[34] Q. Leng, P. Scaria, J. Zhu, N. Ambulos, P. Campbell, and A. J. Mixson, "Highly branched HK peptides are effective carriers of siRNA," *J. Gene Med.*, vol. 7, no. 7, pp. 977–986, 2005.

[35] Q.-R. Chen, L. Zhang, P. W. Luther, and a J. Mixson, "Optimal transfection with the HK polymer depends on its degree of branching and the pH of endocytic vesicles.," *Nucleic Acids Res.*, vol. 30, no. 6, pp. 1338–45, 2002.

[36] Q. Leng, P. Scaria, O. B. Ioffe, M. Woodle, and A. J. Mixson, "A branched histidine/lysine peptide, H2K4b, in complex with plasmids encoding antitumor proteins inhibits tumor xenografts.," *J. Gene Med.*, vol. 8, no. 12, pp. 1407–15, Dec. 2006.

[37] M. X. Tang and F. C. Szoka, "The influence of polymer structure on the interactions of cationic polymers with DNA and morphology of the resulting complexes.," *Gene Ther.*, vol. 4, no. February, pp. 823–832, 1997.

[38] Q. Leng, S.-T. Chou, P. V Scaria, M. C. Woodle, and a J. Mixson, "Buffering capacity and size of siRNA polyplexes influence cytokine levels.," *Mol. Ther.*, vol. 20, no. 12, pp. 2282–90, 2012.

[39] S. Rana, A. Bajaj, R. Mout, and V. M. Rotello, "Monolayer coated gold nanoparticles for delivery applications," *Adv. Drug Deliv. Rev.*, vol. 64, no. 2, pp. 200–216, 2012.

[40] P. S. Ghosh, C. K. Kim, G. Han, N. S. Forbes, and V. M. Rotello, "Efficient gene delivery vectors by tuning the surface charge density of amino acid-functionalized gold nanoparticles," *ACS Nano*, vol. 2, no. 11, pp. 2213–2218, 2008.

[41] S. T. Kim, A. Chompoosor, Y. C. Yeh, S. S. Agasti, D. J. Solfiell, and V. M.

Rotello, “Dendronized gold nanoparticles for siRNA delivery,” *Small*, vol. 8, no. 21, pp. 3253–3256, 2012.
[42] S. Zhang, J. Li, G. Lykotrafitis, G. Bao, and S. Suresh, “Size-Dependent Endocytosis of Nanoparticles,” *Adv. Mater.*, vol. 21, no. 4, pp. 419–424, Jan. 2009.
[43] S. Prabha, W. Z. Zhou, J. Panyam, and V. Labhasetwar, “Size-dependency of nanoparticle-mediated gene transfection: Studies with fractionated nanoparticles,” *Int. J. Pharm.*, vol. 244, no. 1–2, pp. 105–115, 2002.
[44] Q. Leng, J. Kahn, J. Zhu, P. Scaria, and J. Mixson, “Needle-like morphology of H2K4b polyplexes associated with increases in transfection in vitro.,” *Cancer Ther.*, vol. 5B, pp. 193–202, Jun. 2007.
[45] M. Männistö, S. Vanderkerken, V. Toncheva, M. Elomaa, M. Ruponen, E. Schacht, and A. Urtti, “Structure-activity relationships of poly(L-lysines): Effects of pegylation and molecular shape on physicochemical and biological properties in gene delivery,” *J. Control. Release*, vol. 83, no. 1, pp. 169–182, 2002.
[46] Y. P. Ho, C. L. Grigsby, F. Zhao, and K. W. Leong, “Tuning physical properties of nanocomplexes through microfluidics-assisted confinement,” *Nano Lett.*, vol. 11, no. 5, pp. 2178–2182, 2011.
[47] C. M. Goodman, N. S. Chari, G. Han, R. Hong, P. Ghosh, and V. M. Rotello, “DNA-binding by functionalized gold nanoparticles: Mechanism and structural requirements,” *Chem. Biol. Drug Des.*, vol. 67, no. 4, pp. 297–304, 2006.
[48] P. S. Ghosh, G. Han, B. Erdogan, O. Rosado, S. A. Krovi, and V. M. Rotello, “Nanoparticles featuring amino acid-functionalized side chains as DNA receptors,” *Chem. Biol. Drug Des.*, vol. 70, no. 1, pp. 13–18, 2007.
[49] S. D. Solares, J. Chang, J. Seog, and A. U. Kareem, “Utilization of simple scaling laws for modulating tip-sample peak forces in atomic force microscopy characterization in liquid environments,” *J. Appl. Phys.*, vol. 110, no. 9, 2011.
[50] H. Boroudjerdi, A. Naji, and R. R. Netz, “Salt-modulated structure of polyelectrolyte-macroion complex fibers,” *Eur. Phys. J. E*, vol. 34, no. 7, pp. 24–29, 2011.
[51] L. Arcesi, G. La Penna, and A. Perico, “Generalized electrostatic model of the wrapping of DNA around oppositely charged proteins.,” *Biopolymers*, vol. 86, no. 2, pp. 127–35, Jun. 2007.
[52] M. Bezanilla, S. Manne, D. E. Laney, Y. L. Lyubchenko, and H. G. Hansma, “Adsorption of DNA to Mica, Silylated Mica, and Minerals: Characterization by Atomic Force Microscopy,” *Langmuir*, vol. 11, no. 2, pp. 655–659, Feb. 1995.
[53] W. T. Godbey, K. K. Wu, and A. G. Mikos, “Size matters: molecular weight affects the efficiency of poly(ethylenimine) as a gene delivery vehicle.,” *J. Biomed. Mater. Res.*, vol. 45, no. 3, pp. 268–75, Jun. 1999.
[54] M. Breunig, U. Lungwitz, R. Liebl, and A. Goepferich, “Breaking up the correlation between efficacy and toxicity for nonviral gene delivery.,” *Proc. Natl. Acad. Sci. U. S. A.*, vol. 104, no. 36, pp. 14454–9, Sep. 2007.
[55] I. Y. Perevyazko, M. Bauer, G. M. Pavlov, S. Hoeppener, S. Schubert, D. Fischer, and U. S. Schubert, “Polyelectrolyte complexes of DNA and linear

PEI: Formation, composition and properties," *Langmuir*, vol. 28, no. 46, pp. 16167–16176, 2012.

[56] T. Bettinger, J. S. Remy, and P. Erbacher, "Size reduction of galactosylated PEI/DNA complexes improves lectin-mediated gene transfer into hepatocytes," *Bioconjug. Chem.*, vol. 10, no. 4, pp. 558–561, 1999.

[57] R. Golan, L. I. Pietrasanta, W. Hsieh, and H. G. Hansma, "DNA toroids: Stages in condensation," *Biochemistry*, vol. 38, no. 42, pp. 14069–14076, 1999.

[58] Y. Li, U. H. Yildiz, K. Mullen, and F. Gr??hn, "Association of DNA with multivalent organic counterions: From flowers to rods and toroids," *Biomacromolecules*, vol. 10, no. 3, pp. 530–540, 2009.

[59] V. A. Bloomfield, "DNA condensation by multivalent cations.," *Biopolymers*, vol. 44, no. 3, pp. 269–82, 1997.

[60] S. Choosakoonkriang, B. A. Lobo, G. S. Koe, J. G. Koe, and C. R. Middaugh, "Biophysical characterization of PEI/DNA complexes," *J. Pharm. Sci.*, vol. 92, no. 8, pp. 1710–1722, 2003.

[61] Q. Leng and A. J. Mixson, "Modified branched peptides with a histidine-rich tail enhance in vitro gene transfection.," *Nucleic Acids Res.*, vol. 33, no. 4, p. e40, 2005.

[62] Q.-R. Chen, L. Zhang, S. A. Stass, and A. J. Mixson, "Co-polymer of histidine and lysine markedly enhances transfection efficiency of liposomes," *Gene Ther.*, vol. 7, no. 19, pp. 1698–1705, Oct. 2000.

[63] R. Greenwood and K. Kendall, "Selection of Suitable Dispersants for Aqueous Suspensions of Zirconia and Titania Powders using Acoustophoresis," *J. Eur. Ceram. Soc.*, vol. 19, no. 4, pp. 479–488, 1999.

[64] Q. Leng, S.-T. Chou, P. V Scaria, M. C. Woodle, and A. J. Mixson, "Increased tumor distribution and expression of histidine-rich plasmid polyplexes.," *J. Gene Med.*, vol. 16, no. 9–10, pp. 317–28, 2014.

[65] F.-H. Chang, C.-H. Lee, M.-T. Chen, C.-C. Kuo, Y.-L. Chiang, C.-Y. Hang, and S. Roffler, "Surfection: a new platform for transfected cell arrays," *Nucl. Acids Res.*, vol. 32, no. 3, p. e33-, 2004.